

# 000 001 TOAST : TRANSFORMER OPTIMIZATION USING 002 ADAPTIVE AND SIMPLE TRANSFORMATIONS 003 004

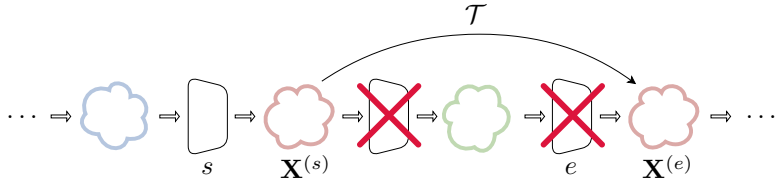
005 **Anonymous authors**

006 Paper under double-blind review

## 007 008 ABSTRACT 009

010 Foundation models achieve State-of-the-art (SOTA) performance across different  
011 tasks, but their size and computational demands raise concerns about accessibility  
012 and sustainability. Existing efficiency methods often require additional retraining  
013 or fine-tuning, limiting their practicality. Recent findings suggest that deep neural  
014 networks exhibit internal representation similarities. While such similarities across  
015 different models have been exploited for enabling techniques such as model stitching  
016 and merging, intra-network redundancy remains underexplored as a source for  
017 efficiency gains. In this paper, we introduce Transformer Optimization using  
018 Adaptive and Simple Transformations (TOAST), a framework that exploits these re-  
019 dundancies to approximate entire transformer blocks with lightweight closed-form  
020 mappings, such as linear transformation or even the identity, without any additional  
021 training. Across SOTA pretrained vision models (e.g., ViT, DINOv2, DeiT) and  
022 datasets ranging from MNIST to ImageNet-1k, TOAST reduces parameters and  
023 computation while preserving, and in some cases improving, downstream perfor-  
024 mance. These results show that large portions of transformer depth can be replaced  
025 by trivial functions, opening a new perspective on efficient foundation models.

## 026 1 INTRODUCTION



027  
028 **Figure 1: Framework Description.** Given two latent spaces  $\mathbf{X}^{(s)}$  and  $\mathbf{X}^{(e)}$  corresponding to  
029 the outputs of blocks  $s$  and  $e$  for a random subset of 500 training samples, TOAST estimates  
030 a lightweight transformation  $\mathcal{T}$  such that  $\mathbf{X}^{(e)} \approx \mathcal{T}(\mathbf{X}^{(s)})$ . This allows *entire* transformer blocks to be  
031 approximated by simple closed-form mappings (e.g., linear or identity), reducing parameters and  
032 computation without retraining.

033 As Neural Networks (NNs) continue to grow in size and complexity, their demand for computational  
034 resources has become a critical bottleneck. While larger models consistently achieve SOTA perfor-  
035 mance, this comes at the cost of substantial memory usage and power consumption, limiting their  
036 accessibility and deployment. This challenge is for instance most relevant in on-device scenarios,  
037 where saving memory, latency, and energy, even by little margins, is critical (Pan et al., 2022; Li et al.,  
038 2022). This has motivated a growing body of work on reducing model complexity. However, most  
039 existing approaches either require additional, resource-intensive training phases or lead to significant  
040 drops in accuracy. Recent studies reveal that there exists strong representational similarities both  
041 within and between NNs. In other words, when focusing on intra-network similarities, different  
042 blocks often perform overlapping functions or produce highly correlated outputs.

043 This redundancy suggests an opportunity: *instead of retraining or pruning, can we approximate these*  
044 *blocks with simpler transformations?* To address this question, we propose Transformer Optimization  
045 using Adaptive and Simple Transformations (TOAST), a novel framework that exploits block-level  
046 representational redundancy to replace transformer blocks with lightweight transformations. By

054 doing so, TOAST reduces parameter count and computational cost, while maintaining (and in some  
 055 cases even improving) downstream task performance. Crucially, our method is training-free, making  
 056 it simple, efficient, and widely applicable, even in resource-constrained scenarios such as deployment  
 057 on edge devices, where even the smallest available models may exceed memory or power budgets.  
 058 Our main contributions are as follows:

- 060 • We propose TOAST, a simple yet effective framework that replaces transformer blocks with  
 061 lightweight transformations (e.g., linear maps or even the identity), significantly reducing  
 062 parameters and computational cost while preserving downstream performance (Figure 1).
- 063 • We introduce linear approximation error as a stable and computationally lightweight criterion  
 064 for identifying redundant transformer blocks (Tables 9 and 11 and Algorithms 1 and 2) and  
 065 we present a systematic analysis of block-wise representational similarities in pre-trained  
 066 vision transformers, revealing consistent redundancy patterns across diverse models and  
 067 motivating the possibility of approximating entire blocks (Figures 2 and 6).
- 068 • We empirically demonstrate that accurate block approximations can be obtained from only a  
 069 few hundred samples, showing that block redundancy can be exploited without requiring  
 070 large-scale retraining (Tables 1 and 4 and Figure 5).
- 071 • We extensively validate our approach across a wide spectrum of vision models (e.g.,  
 072 DiNO-B, ViT-L, DeiT-S, ViT-S, DiNO-S, ViT-T) and datasets ranging from MNIST  
 073 to ImageNet1k, confirming both the generality and efficiency of the method (Tables 1  
 074 to 3 and 12 to 16).
- 075 • We preliminarily validate the application of TOAST beyond vision classification, including  
 076 semantic segmentation using ViT-S and DiNO-B on SceneParse150, and and text  
 077 classification using ModernBERT-B on AG News (Tables 5 and 6 and Section A.2.4).

## 078 2 RELATED WORK

081 **Measuring Similarities** A range of metrics have been introduced to assess the similarity between  
 082 latent spaces generated by different NNs (Klabunde et al., 2023; Ballester et al., 2023). One  
 083 established approach is Canonical Correlation Analysis (CCA) (Hotelling, 1992), known for its  
 084 invariance to linear transformations. Variants of CCA, such as Singular Value CCA (SVCCA) (Raghu  
 085 et al., 2017), aim to enhance robustness, while techniques like Projection Weighted CCA (PWCCA)  
 086 (Morcos et al., 2018) mitigate sensitivity to small perturbations. Another widely used metric, Centered  
 087 Kernel Alignment (CKA) (Kornblith et al., 2019), captures the similarity between latent spaces while  
 088 ignoring orthogonal transformations. However, recent work (Davari et al., 2022) highlights that this  
 089 metric can be sensitive to shifts in the latent space. Additionally, Barannikov et al. (2021) proposes a  
 090 method to compare two data representations by measuring the multi-scale topological dissimilarity,  
 091 while Fumero et al. (2024) leverages the principles of spectral geometry to model and analyze the  
 092 relationships between distinct latent spaces.

093 **Leveraging Similarities** Valeriani et al. (2024) examines the intrinsic dimensionality and neighbor  
 094 compositions of representations in transformer models. Kvigne et al. (2022) investigates how  
 095 models process variations in data points across layers, while Nguyen et al. (2020) assesses the  
 096 impact of network depth and width on hidden representations. Additionally, Crisostomi et al. (2023)  
 097 studies the conditions under which two latent spaces can be merged into a unified one. Moschella  
 098 et al. (2023) constructs a unified space shared by different NNs, enabling zero-shot stitching of  
 099 independently trained models across different modalities (Norelli et al., 2023). More recently,  
 100 Cannistraci et al. (2024) enables model stitching without explicit assumptions about the transformation  
 101 class connecting the latent manifold embeddings, or with only partial correspondence between latent  
 102 spaces (Cannistraci et al., 2023). Finally, Lähner & Moeller (2024); Maiorca et al. (2024) demonstrate  
 103 that representations learned by distinct NNs can be aligned using simple transformations.

104 **Architectural Efficiency** While large-scale models with billions or even trillions of parameters  
 105 continue to achieve state-of-the-art performance, their growth comes with trade-offs, such as slower  
 106 inference times and significantly higher computational costs. Improving the efficiency of Deep Neural  
 107 Network (DNN) has been a long-standing area of research. For instance, Veit et al. (2016) shows  
 108 that removing residual blocks from deep Convolutional Neural Networks (CNNs) only marginally

108 impacts performance, which inspired approaches to reduce inference time by dynamically deciding  
 109 which layers to execute based on the input (Wu et al., 2018; Veit & Belongie, 2018). Additionally,  
 110 various techniques to enhance efficiency have emerged, such as early exiting and model pruning.  
 111 Early exit strategies, which introduce intermediate output layers at different stages of the network,  
 112 have been shown to reduce inference time (Xin et al., 2020; Zhou et al., 2020; Yu et al., 2022; Tang  
 113 et al., 2023). However, these approaches require the training of intermediate classifiers to enable exits  
 114 at predefined layers. Alternatively, model pruning reduces computational load by either removing  
 115 individual weights based on specific criteria, such as gradient information (Ma et al., 2023), entropy  
 116 (Liao et al., 2023), or second-order information (Singh & Alistarh, 2020), or by eliminating larger  
 117 structural components, like channels or residual blocks in ResNets (Bai et al., 2023; Wang & Wu,  
 118 2023), weights in LLMs (Sun et al., 2023) and self-attention layers in Transformers (Zhang & He,  
 119 2020; Sajjad et al., 2023; Venkataramanan et al., 2024; Zhang et al., 2024). Although effective, these  
 120 approaches require training the model from scratch and, in the best case, fine-tuning. However, Bai  
 121 et al. (2023) shows that for CNNs, this additional training step can sometimes be avoided.  
 122

123 Unlike other methods, TOAST leverages intra-network similarities to reduce vision transformers  
 124 complexity *without the need for additional training steps* while maintaining competitive performance.  
 125

### 3 BLOCKS APPROXIMATION

127 The central idea of our approach is that it is possible to leverage representation similarities within  
 128 transformer-based architectures to replace entire blocks with simpler transformations. In this work,  
 129 a *block* refers to a sequence of layers including multi-head self-attention, normalization, and feed-  
 130 forward layers, that function together as a cohesive unit. By replacing these blocks with simpler  
 131 transformations, we can reduce the computational complexity of the network while maintaining its  
 132 core functionality.

133 **Approximating Transformer Blocks** Given two blocks  $s$  and  $e$ , our goal is to replace the interme-  
 134 diate blocks  $s+1, \dots, e$  with a single, lightweight transformation that maps the output of block  $s$   
 135 directly to an approximation of the output of block  $e$ . This approach allows us to skip the computation  
 136 of blocks  $s+1, \dots, e$ , effectively reducing the overall computational costs. This approximation can  
 137 be repeated for multiple, non-overlapping blocks, i.e., blocks  $(s_i, e_i)$  and  $(s_j, e_j)$  with  $e_i < s_j$ . An  
 138 overview of the method is provided in Figure 1.  
 139

140 Let  $\mathbf{X}^{(s)} \in \mathbb{R}^{|\mathcal{D}_{\text{sub}}| \times d_s}$  and  $\mathbf{X}^{(e)} \in \mathbb{R}^{|\mathcal{D}_{\text{sub}}| \times d_e}$  represent the output representations from block  $s$  and  $e$   
 141 respectively, for the data points in  $\mathcal{D}_{\text{sub}} \subset \mathcal{D}$ , sampled uniformly at random from the full training  
 142 dataset  $\mathcal{D}$ . Our objective is to find a transformation  $\mathcal{T} : \mathbb{R}^{d_s} \rightarrow \mathbb{R}^{d_e}$  such that:

$$\mathbf{X}^{(e)} \approx \mathcal{T}(\mathbf{X}^{(s)})$$

145 In this work, we consider  $\mathcal{T}$  to be the *identity* or a *linear transformation*  $\mathbf{T}$ . We can compute the  
 146 linear transformation  $\mathbf{T}$  by minimizing the squared error between the transformed output  $\mathcal{T}(\mathbf{X}^{(s)})$   
 147 and the actual  $\mathbf{X}^{(e)}$ :

$$\mathbf{T} = \arg \min_{\mathcal{T}} \|\mathbf{X}^{(e)} - \mathcal{T}(\mathbf{X}^{(s)})\|_2^2$$

148 This optimization problem allows for a closed-form solution that efficiently computes the optimal  
 149 transformation  $\mathbf{T}$ . The solution bypasses the computation of *all* layers between any two blocks  $s$  and  
 150  $e$ , replacing them with  $\mathbf{T}$ . This approximation reduces computational complexity while minimally  
 151 affecting internal representations, as illustrated in Figures 7 to 11, and preserves compatibility with  
 152 downstream classifiers, achieving significant compression as shown in Tables 1 to 3 and 12 to 15.  
 153

154 **Patterns of Similarity between Transformer Blocks** Inspired by existing results Venkataramanan  
 155 et al. (2024), which show that multi-head attention modules exhibit similarity in learned representa-  
 156 tions, we investigate whether pre-trained foundation models contain *entire blocks* that produce highly  
 157 similar representations. Rather than using CKA to measure representational similarity, we quantify  
 158 how well the output of a later block can be reconstructed from an earlier one using a simple linear  
 159 transformation. All representations are computed using only the [CLS] token, providing a consistent  
 160 and semantically aligned basis for comparing blocks.  
 161

Given representations  $\mathbf{H}_s$  and  $\mathbf{H}_e$  extracted from blocks  $s < e$ , we learn the optimal linear map  $\mathbf{W}^*$  that solves

$$\mathbf{W}^* = \arg \min_{\mathbf{W}} \|\mathbf{H}_e - \mathbf{H}_s \mathbf{W}\|_F^2.$$

We measure similarity via the normalized residual error

$$\epsilon(s, e) = \frac{\|\mathbf{H}_e - \mathbf{H}_s \mathbf{W}^*\|_F}{\|\mathbf{H}_e\|_F},$$

where lower values indicate that block  $e$ 's representations are well explained by a linear transformation of block  $s$ .

By computing the metric for all block pairs, using only a small random subset of the training data (i.e., 50 samples), and ranking them, we can automatically identify blocks whose computations contribute minimally beyond a near-linear mapping. We additionally perform an ablation study comparing several candidate similarity metrics for block selection, and we report these results in Section A.1.3. The procedure used to automatically extract the top- $k$  skip candidates is summarized in Algorithm 1, and the linear approximation error is detailed in Algorithm 2.

## 4 EXPERIMENTS

In this section, we first analyze the similarities between different transformer blocks to motivate their approximation using simple transformations. We then present comprehensive results on image classification across various models and datasets to demonstrate the effectiveness and efficiency of the proposed method. Beyond these core results, we further study the robustness of TOAST through ablations on the number of samples required for approximation and the choice of translator architecture. Overall, our findings show that TOAST achieves strong performance while producing lighter and faster models. Due to space constraints, additional results on zero-shot image classification, as well as further qualitative and quantitative analyses, are provided in the Appendix (Sections A.2.2 and A.2.3).

### 4.1 LATENT ANALYSIS

In this section we investigate similarities in the latent representations of DiNO-B and DEiT-S on five datasets: CIFAR-10, CIFAR-100, MNIST, F-MNIST, and ImageNet1k. We compute the linear approximation error using only the [CLS] token, averaged over a small subset of 50 training samples. This is sufficient to reveal block-level similarity patterns while remaining computationally efficient. Additional results with other pretrained vision transformers (ViT-T, ViT-S, DiNO-S, ViT-B) are provided in Section A.2.1, showing consistent patterns for each model across different datasets.

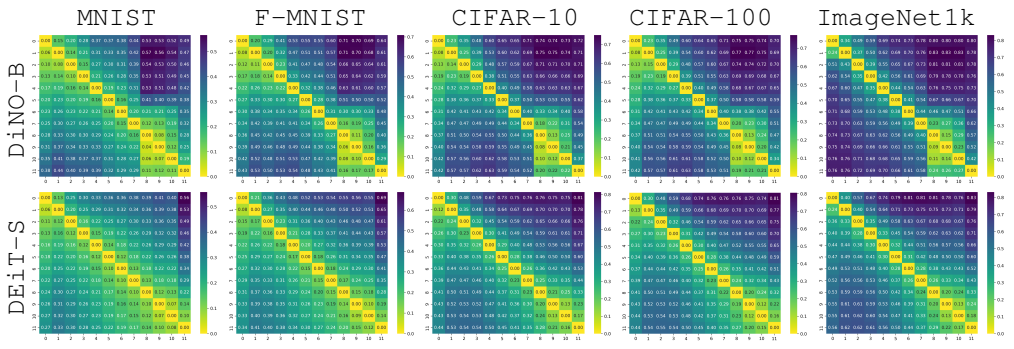


Figure 2: **Block Similarities.** Block-by-block similarities in DiNO-B, and DEiT-S models across five datasets: MNIST, F-MNIST, CIFAR-10, CIFAR-100 and ImageNet1k. Each matrix quantifies the linear approximation error using only the [CLS] token, averaged over a small subset of 50 training samples. The matrices reveal that the similarity between blocks is predominantly influenced by the model rather than the specific dataset. Additional results in Section A.2.1.

**Do vision transformer models exhibit block-wise similarity patterns?** The results in Figure 2 reveal that while the similarity patterns differ across models, they remain largely consistent for the same model across different datasets. This suggests that the similarity structure between computational blocks is predominantly influenced by the model itself. Although the general similarity pattern remains the same, the differences in values become more pronounced (i.e., the block structure becomes more evident) as the complexity of the dataset increases (e.g., from MNIST to ImageNet1k). These findings align with observations from Nguyen et al. (2020), where DNN trained from scratch exhibit a distinctive "block structure" in their representations, which is linked to model overparameterization. Our results extend this observation to vision pre-trained foundation models, showing that such a structure is primarily an intrinsic property of the model. Moreover, these consistent block-wise patterns indicate potential targets for approximation, suggesting that entire blocks may be replaced with simpler transformations without substantially altering the model's internal representations.

**Takeaway** Pre-trained vision foundation models present block-wise similarity patterns that are primarily determined by the model itself.

**How does TOAST affect latent representations?** We next analyze the impact of the proposed transformations on the final block’s latent representations, which are used for downstream classification.

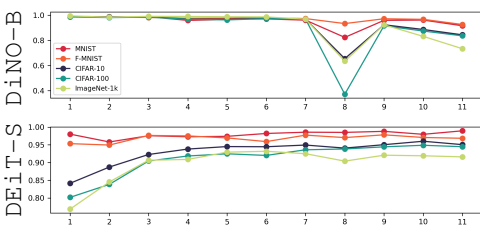
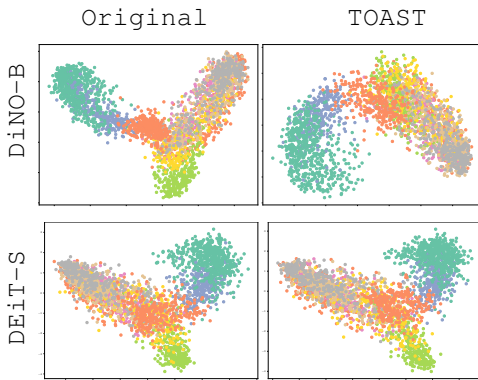


Figure 3: **Approximation vs. Representation Similarity.** CKA between the last block representations of the original and the approximated model when approximating the  $i^{\text{th}}$  block.



**Figure 4: PCA Visualization.** Final block representations for original and TOAST models on F-MNIST reveal DiNO-B’s stronger reliance on final block compared to DEiT-S.

These observations align with the CKA analysis in Figure 3, highlighting that the effect of block approximation depends strongly on the model and its internal block structure. Additional results across other models and datasets are provided in Section A.2.1.

We approximate these blocks using a shared linear transformation applied across all tokens, estimated on a subset of 500 training samples. For consistency, we use the same models and datasets as in Figure 2. To quantify the effect of the approximation, following (Venkataraman et al., 2024; Kornblith et al., 2019) we compute the CKA similarity between the final block representations of the original and the TOAST-approximated model for each block  $k$  using its preceding block as input. As shown in Figure 3, the model-specific similarity patterns re-emerge after approximation. The plots highlight more specific trends. Approximating blocks is easier on simpler tasks (e.g., image classification on MNIST or F-MNIST), yielding representations that closely match the originals, whereas on more complex datasets (e.g., ImageNet1k or CIFAR-100), the approximated representations deviate more from the original ones. Furthermore, the final blocks of DEiT-S exhibit high similarity, suggesting that approximating these layers preserves the final representations, while earlier blocks remain more critical. To provide a more intuitive view, Figure 4 visualizes the final-layer representations using Principal Component Analysis (PCA). We compare the original representations with those obtained after approximating the final block (10 → 11) using TOAST on F-MNIST, with colors indicating the 10 classes. The visualization confirms that approximating the final block of DINO-B results in noticeable deviations from the original representations, whereas for DEiT-S the approximated representations remain highly similar.

270

**Takeaway** Transformer blocks can be approximated using simple transformations, without  
271 compromising representation fidelity.  
272

273

274

**Can entire transformer blocks be approximated without losing accuracy?** Initial results, reported in Table 1, support the qualitative analysis and empirically demonstrate that *entire vision transformer blocks* can be effectively approximated using simpler transformations (e.g., linear projections or, in some cases, the identity function). Such approximations reduce both the number of parameters and Giga Floating-Point Operations (GFLOPs), thereby improving throughput (images per second), while incurring only a slight to negligible decrease in downstream task performance. For instance, consistent with our earlier analysis, we find that approximating the final block of DEiT-S when using ImageNet1k (e.g., approximating blocks  $10 \rightarrow 11$  or  $9 \rightarrow 11$  with a linear transformation) yields modest performance drops going from 73.85% to 73.78% and 70.01%, respectively, while providing substantial efficiency gains. Importantly, we also show that even the identity transformation, achieves competitive results, with accuracy drops as small as -0.24% and -5.44%, respectively. However, the choice of translator naturally depends on the efficiency-accuracy trade-off: linear translation guarantee in general most reliable accuracy-efficiency balance, whereas the identity yields the leanest training-free approximation when maximum simplicity is required. Further methodological details and the full evaluation are presented in Section A.1 and Section 4.2 respectively, while details on the efficiency metrics and additional analysis on those are in Sections A.1.7 and A.2.6, respectively.

289

290

291

292

293

**Table 1: TOAST Image Classification Performance.** Performance comparison using the Identity translator and the Linear Translator for DEiT-S and ImageNet1k across 3 seeds. The "Approx." column specifies the blocks used for approximation, the first one represents the block whose output is used to approximate the second block's output. Additional results in Tables 2 and 3 and Section A.2.2.

Approx.	Params.	Identity Translator			Linear Translator		
		Accuracy % $\uparrow$	GFLOPS $\downarrow$	imgs/s $\uparrow$	Accuracy % $\uparrow$	GFLOPS $\downarrow$	imgs/s $\uparrow$
$2 \rightarrow 4$	-3.25M	$63.74 \pm 0.19(-13.69\%)$	4.15	7222.5	$69.87 \pm 0.14(-5.39\%)$	4.18	7187.6
$9 \rightarrow 11$	-3.25M	$69.83 \pm 0.33(-5.44\%)$	4.15	7224.6	$70.01 \pm 0.27(-5.20\%)$	4.18	7203.8
$0 \rightarrow 1$	-1.62M	$64.02 \pm 0.08(-13.31\%)$	4.56	6755.8	$62.32 \pm 0.15(-15.61\%)$	4.59	6748.9
$10 \rightarrow 11$	-1.62M	$73.67 \pm 0.26(-0.24\%)$	4.56	6751.7	$73.78 \pm 0.28(-0.10\%)$	4.59	6756.3
original	21.81M	$73.85 \pm 0.39$	4.97	6349.2	$73.85 \pm 0.39$	4.97	6325.6

**Takeaway** TOAST effectively reduces model parameters and improve model efficiency without significantly compromising the downstream task performance.

## 4.2 IMAGE CLASSIFICATION PERFORMANCE

We evaluate TOAST on image classification tasks using pretrained models of varying sizes (ViT-L, DiNO-B, and DEiT-S) and two benchmark datasets (CIFAR-100F and ImageNet1k). Additional results with a broader set of models (ViT-T, ViT-S, ViT-B, ViT-L, DiNO-S, DiNO-B, DEiT-S) and datasets (MNIST, F-MNIST, CIFAR-10, CIFAR-100C) are provided in Section A.2.2. While in Section A.2.7, we complement the quantitative evaluations with qualitative analyses of misclassifications after block approximation, providing further insight into model behavior under TOAST. Additional implementation details, including model and dataset specifications, computational resources, and software tools, are provided in Tables 7 and 8, and Sections A.1.5 to A.1.7.

Block approximations in TOAST are calculated via a shared linear, or identity, transformation applied across all tokens and are estimated using a subset of 500 training samples. A linear classifier is then trained on top of the frozen backbone with the Adam optimizer (learning rate 0.001), batch size 256, for 5 epochs, over 3 different seeds. This setup simulates a realistic scenario where a pretrained feature extractor is adapted to a new dataset unseen during pretraining. However, to assess the robustness of our method, we also report the results using the original classification heads (Section A.2.5), which confirm the consistency of our findings.

**Are TOAST results competitive?** As shown in Tables 2 and 3, TOAST consistently reduces model size and GFLOPs while maintaining, and in some cases improving, image classification

324 **Table 2: TOAST Classification Performance on ImageNet1k.** Image classification accuracy,  
 325 GFLOPs, and throughput for DEiT-S, DiNo-B, and ViT-L using ImageNet1k. The "Approx."  
 326 column indicates the block pairs where the first block approximates the second. Additional results  
 327 using other models and datasets are provided in Table 3 and Section A.2.2.

	Approx.	Params.	Identity			Linear		
			Accuracy % $\uparrow$	GFLOPs $\downarrow$	imgs/s $\uparrow$	Accuracy % $\uparrow$	GFLOPs $\downarrow$	imgs/s $\uparrow$
DEiT-S	3 $\rightarrow$ 4, 9 $\rightarrow$ 11	-4.88M	66.96 $\pm$ 0.34(-9.33%)	3.74	7751.4	68.39 $\pm$ 0.13(-7.39%)	3.80	7718.4
	3 $\rightarrow$ 4, 9 $\rightarrow$ 10	-3.25M	69.22 $\pm$ 0.13(-6.27%)	4.15	7210.9	71.35 $\pm$ 0.22(-3.38%)	4.21	7188.4
	2 $\rightarrow$ 3	-1.62M	70.80 $\pm$ 0.05(-4.12%)	4.56	6754.2	73.19 $\pm$ 0.19(-0.88%)	4.59	6736.7
	10 $\rightarrow$ 11	-1.62M	<b>73.67 <math>\pm</math> 0.26(-0.24%)</b>	4.56	6752.6	<b>73.78 <math>\pm</math> 0.28(-0.09%)</b>	4.59	6740.5
	original	21.81M	73.85 $\pm$ 0.39	4.97	6349.2	73.85 $\pm$ 0.39	4.97	6325.6
DiNo-B	0 $\rightarrow$ 4	-26.00M	3.58 $\pm$ 0.06(-95.20%)	16.32	3230.9	27.70 $\pm$ 0.19(-62.71%)	16.47	3227.7
	0 $\rightarrow$ 1, 2 $\rightarrow$ 3, 4 $\rightarrow$ 5	-19.50M	6.98 $\pm$ 0.18(-90.63%)	18.34	2947.0	61.02 $\pm$ 0.36(-17.86%)	18.80	2929.6
	0 $\rightarrow$ 1, 2 $\rightarrow$ 3	-13.00M	13.28 $\pm$ 0.46(-82.18%)	20.37	2703.9	70.82 $\pm$ 0.49(-4.66%)	20.67	2681.2
	0 $\rightarrow$ 1	-6.50M	<b>65.47 <math>\pm</math> 0.43(-12.14%)</b>	22.39	2506.6	<b>73.43 <math>\pm</math> 0.02(-1.15%)</b>	22.54	2487.0
	5 $\rightarrow$ 6	-6.50M	28.84 $\pm$ 0.51(-61.30%)	22.39	2503.1	73.01 $\pm$ 0.41(-1.71%)	22.54	2490.6
ViT-L	original	86.58M	74.52 $\pm$ 0.26	24.42	2321.3	74.52 $\pm$ 0.26	24.42	2316.5
	2 $\rightarrow$ 4, 18 $\rightarrow$ 23	-80.83M	62.92 $\pm$ 0.21(-19.89%)	45.05	1654.9	67.43 $\pm$ 0.05(-14.16%)	45.47	1652.8
	17 $\rightarrow$ 23	-69.28M	66.81 $\pm$ 0.34(-14.95%)	47.70	1572.4	66.87 $\pm$ 0.52(-14.87%)	47.90	1567.0
	3 $\rightarrow$ 4, 19 $\rightarrow$ 23	-57.74M	70.97 $\pm$ 0.42(-9.65%)	50.34	1509.9	71.50 $\pm$ 0.14(-8.98%)	50.75	1499.5
	3 $\rightarrow$ 4, 20 $\rightarrow$ 23	-46.19M	73.49 $\pm$ 0.18(-6.44%)	52.98	1440.4	74.03 $\pm$ 0.43(-5.76%)	53.39	1436.8
ViT-L	3 $\rightarrow$ 4, 21 $\rightarrow$ 23	-34.64M	75.80 $\pm$ 0.26(-3.50%)	55.62	1377.2	76.30 $\pm$ 0.14(-2.86%)	56.03	1345.6
	7 $\rightarrow$ 8, 15 $\rightarrow$ 16	-23.09M	76.81 $\pm$ 0.28(-2.21%)	58.26	1318.2	77.32 $\pm$ 0.48(-1.56%)	58.67	1316.4
	16 $\rightarrow$ 17, 22 $\rightarrow$ 23	-23.09M	77.64 $\pm$ 0.32(-1.15%)	58.26	1318.8	77.64 $\pm$ 0.02(-1.16%)	58.67	1312.3
	3 $\rightarrow$ 4	-11.55M	77.32 $\pm$ 0.29(-1.57%)	60.90	1269.2	<b>78.36 <math>\pm</math> 0.26(-0.24%)</b>	61.11	1270.0
	22 $\rightarrow$ 23	-11.55M	<b>78.32 <math>\pm</math> 0.09(-0.29%)</b>	60.90	1267.5	78.21 $\pm$ 0.19(-0.43%)	61.11	1270.9
ViT-L	original	304.35M	78.55 $\pm$ 0.20	63.54	1219.8	78.55 $\pm$ 0.20	63.54	1225.2

accuracy. This aligns with our representational analyses in Section 4.1: for instance, approximating the final block of DEiT-S produces latent representations nearly identical to the original (Figures 3 and 4), making it an ideal candidate for approximation. Even when multiple consecutive blocks are approximated (e.g., 9  $\rightarrow$  11), models maintain performance comparable to or exceeding the original while significantly reducing parameters. This demonstrates that a simple linear transformation, or even the identity in certain cases, is sufficient to capture the functionality of full transformer blocks without additional training, provided the transformation is shared across all tokens.

Table 3: TOAST Classification Performance on CIFAR-100F. Image classification accuracy, GFLOPs, and throughput for DEiT-S, DiNo-B, and ViT-L using CIFAR-100F. The "Approx." column indicates the block pairs where the first block approximates the second. Additional results using other models and datasets are provided in Section A.2.2.

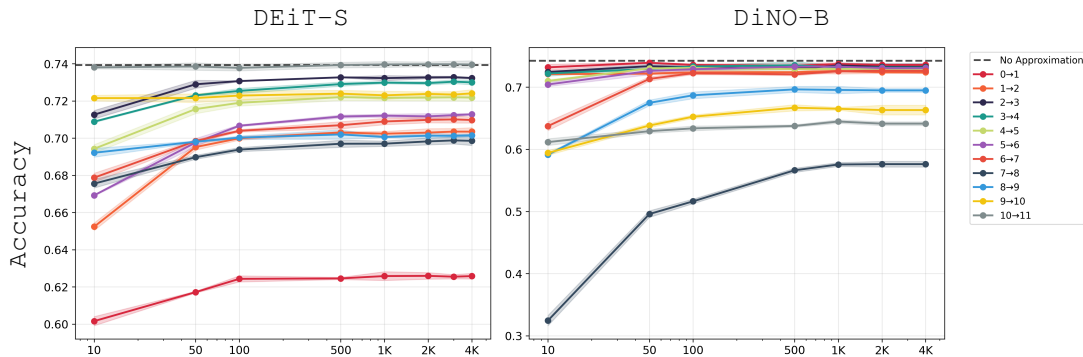
	Approx.	Params.	Identity			Linear		
			Accuracy % $\uparrow$	GFLOPs $\downarrow$	imgs/s $\uparrow$	Accuracy % $\uparrow$	GFLOPs $\downarrow$	imgs/s $\uparrow$
DEiT-S	3 $\rightarrow$ 4, 9 $\rightarrow$ 11	-4.88M	68.48 $\pm$ 0.34(-3.44%)	3.74	7755.1	70.64 $\pm$ 0.37(-0.39%)	3.80	7713.7
	9 $\rightarrow$ 11	-3.25M	<b>72.28 <math>\pm</math> 0.36(+1.92%)</b>	4.15	7226.6	<b>72.04 <math>\pm</math> 0.42(+1.57%)</b>	4.18	6791.7
	8 $\rightarrow$ 9	-1.62M	71.34 $\pm$ 0.10(+0.60%)	4.56	6755.2	70.80 $\pm$ 0.12(-0.17%)	4.59	6739.9
	9 $\rightarrow$ 10	-1.62M	71.66 $\pm$ 0.39(+1.04%)	4.56	6692.1	71.49 $\pm$ 0.20(+0.80%)	4.59	6741.3
	original	21.81M	70.92 $\pm$ 0.18	4.97	6349.0	70.92 $\pm$ 0.18	4.97	6249.4
DiNo-B	0 $\rightarrow$ 4	-26.00M	18.29 $\pm$ 0.86(-79.09%)	16.32	3233.8	62.25 $\pm$ 0.54(-28.83%)	16.47	3204.9
	0 $\rightarrow$ 1, 2 $\rightarrow$ 3, 4 $\rightarrow$ 5	-19.50M	29.05 $\pm$ 0.31(-66.79%)	18.34	2943.1	79.06 $\pm$ 0.27(-9.60%)	18.80	2922.6
	0 $\rightarrow$ 1, 2 $\rightarrow$ 3	-13.00M	33.25 $\pm$ 0.18(-61.99%)	20.37	2705.6	84.18 $\pm$ 0.18(-3.76%)	20.67	2690.1
	0 $\rightarrow$ 1	-6.50M	<b>78.83 <math>\pm</math> 0.22(-9.87%)</b>	22.39	2492.8	<b>86.64 <math>\pm</math> 0.37(-0.94%)</b>	22.54	2493.8
	2 $\rightarrow$ 3	-6.50M	47.51 $\pm$ 0.52(-45.68%)	22.39	2484.2	86.06 $\pm$ 0.20(-1.60%)	22.54	2484.6
ViT-L	original	86.58M	87.46 $\pm$ 0.04	24.42	2315.5	87.46 $\pm$ 0.04	24.42	2317.3
	2 $\rightarrow$ 4, 18 $\rightarrow$ 23	-80.83M	74.41 $\pm$ 0.44(-13.79%)	45.05	1655.7	84.02 $\pm$ 0.39(-2.66%)	45.47	1649.6
	17 $\rightarrow$ 23	-69.28M	85.32 $\pm$ 0.45(-1.16%)	47.69	1578.8	84.55 $\pm$ 0.44(-2.05%)	47.90	1552.1
	3 $\rightarrow$ 4, 19 $\rightarrow$ 23	-57.74M	84.23 $\pm$ 0.08(-2.43%)	50.34	1503.6	85.81 $\pm$ 0.39(-0.59%)	50.75	1497.4
	3 $\rightarrow$ 4, 20 $\rightarrow$ 23	-46.19M	84.68 $\pm$ 0.18(-1.90%)	52.98	1445.2	86.30 $\pm$ 0.11(-0.03%)	53.39	1431.0
ViT-L	20 $\rightarrow$ 23	-34.64M	<b>86.61 <math>\pm</math> 0.07(+0.33%)</b>	55.62	1381.2	86.55 $\pm$ 0.22(+0.27%)	55.82	1372.6
	3 $\rightarrow$ 4, 21 $\rightarrow$ 23	-34.64M	84.86 $\pm$ 0.28(-1.70%)	55.62	1376.7	86.37 $\pm$ 0.28(+0.06%)	56.03	1372.7
	20 $\rightarrow$ 22	-23.09M	86.30 $\pm$ 0.23(-0.03%)	58.26	1317.5	86.52 $\pm$ 0.12(+0.24%)	58.47	1314.6
	3 $\rightarrow$ 4, 21 $\rightarrow$ 22	-23.09M	84.58 $\pm$ 0.19(-2.02%)	58.26	1315.8	86.20 $\pm$ 0.11(-0.14%)	58.67	1317.6
	20 $\rightarrow$ 21	-11.55M	86.44 $\pm$ 0.24(+0.14%)	60.90	1268.5	86.39 $\pm$ 0.08(+0.08%)	61.11	1266.7
ViT-L	21 $\rightarrow$ 22	-11.55M	86.55 $\pm$ 0.01(+0.26%)	60.90	1270.7	<b>86.72 <math>\pm</math> 0.24(+0.46%)</b>	61.11	1269.2
	original	304.35M	86.32 $\pm$ 0.08	63.54	1223.1	86.32 $\pm$ 0.08	63.54	1224.3

Additionally, efficiency gains are notable: throughput (imgs/s) increases while GFLOPs decreases, highlighting practical benefits for deployment, as also shown in Section A.2.6. Additional results

378 across other models (DiNO-B, ViT-L) and datasets confirm that TOAST generalizes across  
 379 architectures and scales (Section A.2.2). Finally, while approximations are easier for simpler datasets  
 380 (e.g., CIFAR-100F), TOAST still achieves meaningful compression with minimal accuracy loss  
 381 on complex datasets like ImageNet1k. Additional results across models and datasets are provided  
 382 in Tables 12 to 15. To assess scalability, we applied TOAST to ViT-L. Approximating selected  
 383 blocks, e.g., 17 → 23, reduces the parameter count by 69.3M, lowers GFLOPs from 63.54 to 47.79,  
 384 and increases throughput from 1223.1 to 1578.8 imgs/s, while incurring a minimal accuracy drop  
 385 of 1.16%. This shows TOAST’s utility in balancing substantial computational savings with a modest  
 386 performance trade-off, even in large models.

387 **Takeaway** Approximating selected blocks enables efficiency gains with minimal impact on  
 388 the accuracy.

391 **Are 500 training samples enough?** We study the sensitivity of block approximation to the number  
 392 of training samples using DiNO-B and DEiT-S on ImageNet1k. As shown in Figure 5, perfor-  
 393 mance typically plateaus quickly: 500 samples are sufficient to obtain stable and reliable approxima-  
 394 tions. Increasing the sample count beyond this threshold provides only marginal gains, while substan-  
 395 tially fewer samples lead to noticeable degradation. Interestingly, when the representational spaces of  
 396 consecutive blocks are already highly aligned, even as few as 10 or 50 samples suffice to achieve com-  
 397 petitive approximations. Conversely, for blocks that are harder to approximate, such as the early layers  
 398 of DEiT-S (e.g., 0→1), even 4000 samples are insufficient to estimate a linear transformation that  
 399 maintains competitive performance. We highlight that these results are obtained on ImageNet1k,  
 400 which contains 1000 classes. The 500 samples represent only a small subset of the class space, yet re-  
 401 liable approximations are still achieved. This indicates that TOAST primarily captures the block-level  
 402 structure of representations rather than requiring exhaustive coverage of all classes. Consequently,  
 403 TOAST could be practical also in scenarios where a large labeled datasets is limited.



415 **Figure 5: Sample Size Ablation.** Classification accuracy as a function of the number of training  
 416 samples used for approximating different layers of DiNO-B and DEiT-S with a linear transformation  
 417 using ImageNet1k. Accuracy stabilizes after approximately 500 samples.

418 **Takeaway** A small number of samples is sufficient to achieve stable and reliable representa-  
 419 tions when approximating transformer blocks, balancing efficiency and accuracy.

423 **What if a more complex transformation is used?** We evaluate whether deeper approximators  
 424 improve downstream task performance. Specifically, we compare TOAST (Identity and Linear)  
 425 to MultiLayer Perceptron (MLP) and Residual MLP, trained for 300 steps with Adam (learning  
 426 rate  $10^{-3}$ ). These more complex transformation, as for Identity and Linear, are applied across all  
 427 tokens, and estimated using a subset of 500 training samples. Results in Table 4 show a consistent  
 428 trend for ViT-L on both ImageNet1k and CIFAR-100F: the linear transformation provides the  
 429 most reliable trade-off across datasets. On CIFAR-100F, linear often achieves the best or near-best  
 430 accuracy (e.g., 21→22: 86.72% vs. 86.82% for Res-MLP and 85.20% for MLP), while remaining  
 431 training-free, thus more efficient. On ImageNet1k, the gap becomes even clearer: for the same  
 blocks linear reaches 77.24%, while Res-MLP and MLP reach 77.14% and 74.20%, respectively.

432 Additionally, also Linear obtain competitive results. TOAST operates in closed form, requires no  
 433 optimization, and consistently achieves strong efficiency–accuracy trade-offs. These findings confirm  
 434 that a simple linear transformation is sufficient to approximate transformer blocks in most settings,  
 435 with deeper translators offering little benefit despite their higher cost.  
 436

437 **Table 4: Transformations Comparison.** Classification accuracy on CIFAR-100F and  
 438 ImageNet1k using ViT-L. The "Approx." column specifies the block mapping (output of the first  
 439 block is used to approximate the output of the second). MLP and Res-MLP are trained approximators,  
 440 while Identity and Linear are closed-form and training-free. Results are averaged over three seeds.

		Accuracy $\uparrow$				
	Approx.	Params.	Identity	Linear	MLP	Res-MLP
CIFAR-100F	3 $\rightarrow$ 4, 20 $\rightarrow$ 23	-46.19M	84.68 $\pm$ 0.18	86.30 $\pm$ 0.11	84.36 $\pm$ 0.48	86.10 $\pm$ 0.39
	17 $\rightarrow$ 23	-69.28M	84.58 $\pm$ 0.19	86.20 $\pm$ 0.11	84.83 $\pm$ 0.31	86.49 $\pm$ 0.08
	3 $\rightarrow$ 4, 19 $\rightarrow$ 23	-57.74M	84.23 $\pm$ 0.08	85.81 $\pm$ 0.39	83.63 $\pm$ 0.42	85.58 $\pm$ 0.06
	20 $\rightarrow$ 23	-34.64M	86.61 $\pm$ 0.07	86.55 $\pm$ 0.22	84.68 $\pm$ 0.39	86.19 $\pm$ 0.02
	3 $\rightarrow$ 4, 21 $\rightarrow$ 23	-34.64M	84.86 $\pm$ 0.28	86.37 $\pm$ 0.28	84.90 $\pm$ 0.71	86.10 $\pm$ 0.37
	20 $\rightarrow$ 22	-23.09M	86.30 $\pm$ 0.23	86.52 $\pm$ 0.12	84.97 $\pm$ 0.18	86.71 $\pm$ 0.28
	3 $\rightarrow$ 4, 21 $\rightarrow$ 22	-23.09M	84.58 $\pm$ 0.19	86.20 $\pm$ 0.11	84.83 $\pm$ 0.31	86.49 $\pm$ 0.08
	20 $\rightarrow$ 21	-11.55M	86.44 $\pm$ 0.24	86.39 $\pm$ 0.08	84.40 $\pm$ 0.70	86.63 $\pm$ 0.06
	21 $\rightarrow$ 22	-11.55M	86.55 $\pm$ 0.01	86.72 $\pm$ 0.24	85.20 $\pm$ 0.26	86.82 $\pm$ 0.31
	original	304.35M	86.32 $\pm$ 0.08	86.32 $\pm$ 0.08	86.32 $\pm$ 0.08	86.32 $\pm$ 0.08
ImageNet1k	3 $\rightarrow$ 4, 20 $\rightarrow$ 23	-46.19M	73.49 $\pm$ 0.18	74.03 $\pm$ 0.43	69.49 $\pm$ 0.24	73.68 $\pm$ 0.12
	17 $\rightarrow$ 23	-69.28M	84.58 $\pm$ 0.19	86.20 $\pm$ 0.11	84.83 $\pm$ 0.31	86.49 $\pm$ 0.08
	3 $\rightarrow$ 4, 19 $\rightarrow$ 23	-57.74M	70.97 $\pm$ 0.42	71.50 $\pm$ 0.14	66.19 $\pm$ 0.17	70.75 $\pm$ 0.07
	20 $\rightarrow$ 23	-34.64M	74.45 $\pm$ 0.07	74.45 $\pm$ 0.24	70.19 $\pm$ 0.30	74.46 $\pm$ 0.22
	3 $\rightarrow$ 4, 21 $\rightarrow$ 23	-34.64M	75.80 $\pm$ 0.26	76.30 $\pm$ 0.14	73.23 $\pm$ 0.29	76.14 $\pm$ 0.22
	20 $\rightarrow$ 22	-23.09M	75.49 $\pm$ 0.19	74.84 $\pm$ 0.21	70.56 $\pm$ 0.25	75.59 $\pm$ 0.18
	3 $\rightarrow$ 4, 21 $\rightarrow$ 22	-23.09M	76.25 $\pm$ 0.02	76.61 $\pm$ 0.29	73.52 $\pm$ 0.40	76.43 $\pm$ 0.21
	20 $\rightarrow$ 21	-11.55M	77.00 $\pm$ 0.27	77.19 $\pm$ 0.25	72.72 $\pm$ 0.31	76.24 $\pm$ 0.21
	21 $\rightarrow$ 22	-11.55M	77.24 $\pm$ 0.28	77.06 $\pm$ 0.24	74.20 $\pm$ 0.48	77.14 $\pm$ 0.27
	original	304.35M	78.55 $\pm$ 0.20	86.32 $\pm$ 0.20	86.32 $\pm$ 0.20	86.32 $\pm$ 0.20

461 **Takeaway** TOAST consistently matches or outperforms deeper trained approximators while  
 462 requiring no gradient-based training.

### 4.3 TOAST APPLICABILITY TO OTHER TASKS OR DOMAINS

466 We further evaluate TOAST beyond vision classification by applying it to text classification and  
 467 semantic segmentation tasks. For text classification, we use ModernBERT-B on the AG News  
 468 dataset, while for segmentation we employ the same backbone on the SceneParse150 dataset.  
 469

470 **Table 5: TOAST Text Classification Performance on AG News.** Text classification accuracy,  
 471 GFLOPs, and throughput for ModernBERT-B using AG News. The "Approx." column specifies  
 472 the block mapping (output of the first block is used to approximate the output of the second). MLP is  
 473 a trained approximators, while Linear is closed-form and training-free. Results are averaged over  
 474 three seeds. Additional results are provided in Section A.2.4.

476	Approx.	Params $\downarrow$	Linear			MLP		
			Accuracy% $\uparrow$	GFLOPs $\downarrow$	img/s $\uparrow$	Accuracy% $\uparrow$	GFLOPs $\downarrow$	token/s $\uparrow$
477	11 $\rightarrow$ 21	92.82M	0.81 $\pm$ 0.05	12.7	2264.0	0.73 $\pm$ 0.00	12.68	2216.50
478	4 $\rightarrow$ 8, 11 $\rightarrow$ 14, 18 $\rightarrow$ 21	92.82M	0.82 $\pm$ 0.07	12.7	2220.7	0.73 $\pm$ 0.01	12.68	2155.16
479	4 $\rightarrow$ 7, 18 $\rightarrow$ 21	109.68M	0.82 $\pm$ 0.07	15.9	1803.9	0.71 $\pm$ 0.02	15.85	1771.80
480	4 $\rightarrow$ 8	126.54M	0.86 $\pm$ 0.02	19.0	1636.0	0.82 $\pm$ 0.01	19.03	1632.65
481	11 $\rightarrow$ 14	132.16M	0.86 $\pm$ 0.02	20.1	1544.3	0.82 $\pm$ 0.01	20.08	1540.23
482	18 $\rightarrow$ 21	132.16M	0.85 $\pm$ 0.02	20.1	1472.8	0.82 $\pm$ 0.01	20.08	1467.56
483	4 $\rightarrow$ 5	143.40M	0.88 $\pm$ 0.00	22.2	1380.3	0.81 $\pm$ 0.01	22.20	1384.42
484	11 $\rightarrow$ 12	143.40M	0.87 $\pm$ 0.02	22.2	1378.8	0.82 $\pm$ 0.01	22.20	1394.63
485	20 $\rightarrow$ 21	143.40M	0.87 $\pm$ 0.02	22.2	1340.2	0.84 $\pm$ 0.00	22.20	1332.27
	original	149.01M	0.88 $\pm$ 0.00	23.25	1337.25	0.88 $\pm$ 0.00	23.25	1347.46

Additional implementation details, including model and dataset specifications, computational resources, and software tools, are provided in Tables 7 and 8 and Sections A.1.5 to A.1.7, with complete results in Section A.2.4. For both domains, we adopt the same setup as in the vision experiments: block approximations are implemented via a shared linear map, identity, or small MLP transformation applied across all tokens, estimated using a subset of 500 training samples. In the text domain, a linear classifier is trained on top of the frozen backbone for 5 epochs over 3 seeds. For segmentation, a segmentation head is trained on the frozen backbone for 10 epochs over 3 seeds. The results in Table 5 show that, in this setting as well, the linear transformation outperforms the more complex MLP. Moreover, up to 10 blocks can be approximated (i.e.,  $11 \rightarrow 21$ ), substantially reducing GFLOPs, improving throughput, and decreasing model size, while incurring only a minimal drop in accuracy. Results in Table 6 further demonstrate that a linear transformation is sufficient even for a more complex task such as segmentation, indicating that appropriately selecting which layers to approximate enables model size reduction with minimal impact on downstream accuracy.

**Takeaway** TOAST extends beyond vision and standard classification, demonstrating broader applicability across domains.

## 5 LIMITATIONS AND FUTURE WORK

While TOAST efficiently approximates transformer blocks, our current investigation has primarily focused on vision transformer architectures and their application to classification tasks with preliminary results also extending to segmentation and text classification. Future research will explore the applicability of TOAST to other modalities and to diverse downstream tasks (e.g., image reconstruction). Such an expansion will be crucial for testing the universality of the observed block-similarity phenomena and assessing TOAST’s adaptability. Furthermore, we aim to expand the analysis of these block-level similarities. This involves investigating redundancies at finer granularities, such as within individual attention heads or feed-forward layers, and consistently developing more principled and reliable metrics for automatically selecting which blocks to approximate. The heuristic used in the current work, while effective, is not yet fully accurate, and improving it could enable more consistent identification of approximation-friendly layers with minimal impact on downstream performance. Such advancements may lead to more refined, context-aware approximation strategies that further enhance model efficiency.

## 6 CONCLUSION

In this work, we first analyze the emergence of consistent block-wise representation similarities within pretrained foundation models and then propose a method to leverage these similarities to obtain smaller and more efficient yet performant models. To this end, we propose Transformer Optimization using Adaptive and Simple Transformations (TOAST), a novel method for easily approximate entire transformer blocks using a simple transformation, without requiring additional training or fine-tuning. Our extensive empirical evaluations across multiple pretrained vision models and datasets validate that TOAST significantly reduces model parameters while maintaining, and sometimes even improving, downstream task performance. Furthermore, TOAST’s straightforward linear approach often achieves better results than existing strategies like block skipping, and can be more effective than complex, trained approximations. TOAST thus offers a practical and efficient method for streamlining foundation models, making them more computationally accessible, and towards deployment in resource-constrained scenarios such as on-device settings.

**Table 6: Segmentation Performance.** mIoU results for each single skip configuration using ViT-S and DiNO-B.

Approx.	mIoU $\uparrow$			
	ViT-S		DiNO-B	
	Linear	MLP	Linear	MLP
$0 \rightarrow 1$	0.27	0.26	0.29	0.29
$1 \rightarrow 2$	0.29	0.29	0.29	0.29
$2 \rightarrow 3$	0.30	0.30	0.29	0.29
$3 \rightarrow 4$	0.30	0.29	0.29	0.29
$4 \rightarrow 5$	0.30	0.29	0.29	0.29
$5 \rightarrow 6$	0.28	0.27	0.29	0.29
$6 \rightarrow 7$	0.28	0.27	0.29	0.29
$7 \rightarrow 8$	0.29	0.28	0.26	0.23
$8 \rightarrow 9$	0.28	0.27	0.28	0.27
$9 \rightarrow 10$	0.29	0.29	0.27	0.26
$10 \rightarrow 11$	0.30	0.29	0.27	0.26
original		0.31		0.29

## 540 ETHICS STATEMENT

541

542 This work adheres to the ICLR Code of Ethics. Our study focuses exclusively on pre-trained vision  
 543 models and publicly available datasets, with no human subjects or sensitive personal data involved.  
 544 All experimental protocols comply with legal, privacy, and ethical standards for AI research. The  
 545 methods proposed in this paper aim solely to improve computational efficiency, without introducing  
 546 harm or enabling misuse.

547

## 548 REPRODUCIBILITY STATEMENT

549

550 To ensure reproducibility, we provide detailed descriptions of all experiments, model configurations,  
 551 datasets, training procedures, and hyperparameters in the main text and Appendix (Sections A.1.5  
 552 to A.1.7 and A.2.2). Additionally, the full implementation of TOAST, including scripts for block  
 553 approximation and evaluation, is included as anonymous supplementary material. All results reported  
 554 in the paper can be reproduced using these resources.

555

## 556 REFERENCES

557

558 Shipeng Bai, Jun Chen, Xintian Shen, Yixuan Qian, and Yong Liu. Unified data-free compression:  
 559 Pruning and quantization without fine-tuning. In *Proceedings of the IEEE/CVF International  
 Conference on Computer Vision*, pp. 5876–5885, 2023.

560

561 Rubén Ballester, Carles Casacuberta, and Sergio Escalera. Topological data analysis for neural  
 562 network analysis: A comprehensive survey. *arXiv preprint arXiv:2312.05840*, December 2023.

563

564 Serguei Barannikov, Ilya Trofimov, Nikita Balabin, and Evgeny Burnaev. Representation topology  
 565 divergence: A method for comparing neural network representations. *arXiv preprint  
 arXiv:2201.00058*, 2021.

566

567 Lucas Beyer, Xiaohua Zhai, and Alexander Kolesnikov. Better plain vit baselines for imagenet-1k,  
 568 2022.

569

570 Irene Cannistraci, Luca Moschella, Valentino Maiorca, Marco Fumero, Antonio Norelli, and  
 571 Emanuele Rodolà. Bootstrapping parallel anchors for relative representations. In Krystal  
 572 Maughan, Rosanne Liu, and Thomas F. Burns (eds.), *The First Tiny Papers Track at ICLR  
 2023, Tiny Papers @ ICLR 2023, Kigali, Rwanda, May 5, 2023*. OpenReview.net, 2023. URL  
 573 <https://openreview.net/pdf?id=VBuUL2IWlq>.

574

575 Irene Cannistraci, Luca Moschella, Marco Fumero, Valentino Maiorca, and Emanuele Rodolà. From  
 576 bricks to bridges: Product of invariances to enhance latent space communication. In *The Twelfth  
 577 International Conference on Learning Representations*, 2024. URL <https://openreview.net/forum?id=vngVydDWft>.

578

579 Donato Crisostomi, Irene Cannistraci, Luca Moschella, Pietro Barbiero, Marco Ciccone, Pietro  
 580 Lio, and Emanuele Rodolà. From charts to atlas: Merging latent spaces into one. In *NeurIPS  
 581 2023 Workshop on Symmetry and Geometry in Neural Representations*, 2023. URL <https://openreview.net/forum?id=ZFu7CPTznY>.

583

584 MohammadReza Davari, Stefan Horoi, Amine Natik, Guillaume Lajoie, Guy Wolf, and Eu-  
 585 gene Belilovsky. Reliability of cka as a similarity measure in deep learning. *arXiv preprint  
 arXiv:2210.16156*, 2022.

586

587 Li Deng. The mnist database of handwritten digit images for machine learning research. *IEEE Signal  
 588 Processing Magazine*, 29(6):141–142, 2012.

589

590 Alexey Dosovitskiy, Lucas Beyer, Alexander Kolesnikov, Dirk Weissenborn, Xiaohua Zhai, Thomas  
 591 Unterthiner, Mostafa Dehghani, Matthias Minderer, Georg Heigold, Sylvain Gelly, Jakob Uszkoreit,  
 592 and Neil Houlsby. An image is worth 16x16 words: Transformers for image recognition at scale.  
 593 In *9th International Conference on Learning Representations, ICLR 2021, Virtual Event, Austria,  
 May 3-7, 2021*. OpenReview.net, 2021. URL <https://openreview.net/forum?id=YicbFdNTTy>.

594 Marco Fumero, Marco Pegoraro, Valentino Maiorca, Francesco Locatello, and Emanuele Rodolà.  
 595 Latent functional maps: a spectral framework for representation alignment. In A. Globerson,  
 596 L. Mackey, D. Belgrave, A. Fan, U. Paquet, J. Tomczak, and C. Zhang (eds.), *Advances in Neural Information Processing Systems*, volume 37, pp. 66178–66203. Curran Asso-  
 597 ciates, Inc., 2024. URL [https://proceedings.neurips.cc/paper\\_files/paper/2024/file/79be41d858841037987964e3f5caf76d-Paper-Conference.pdf](https://proceedings.neurips.cc/paper_files/paper/2024/file/79be41d858841037987964e3f5caf76d-Paper-Conference.pdf).

600 Harold Hotelling. Relations between two sets of variates. *Breakthroughs in statistics: methodology*  
 601 *and distribution*, pp. 162–190, 1992.

602 Max Klabunde, Tobias Schumacher, Markus Strohmaier, and Florian Lemmerich. Similarity of  
 603 neural network models: A survey of functional and representational measures. *arXiv preprint*  
 604 *arXiv:2305.06329*, 2023.

605 Simon Kornblith, Mohammad Norouzi, Honglak Lee, and Geoffrey Hinton. Similarity of neural  
 606 network representations revisited. In *International Conference on Machine Learning*, pp. 3519–  
 607 3529. PMLR, 2019.

608 Alex Krizhevsky, Geoffrey Hinton, et al. Learning multiple layers of features from tiny images. 2009.

609 Ruslan Kuprieiev, skshetry, Dmitry Petrov, Paweł Redzynski, Peter Rowlands, Casper da Costa-  
 610 Luis, Alexander Schepanovski, Ivan Shcheklein, Batuhan Taskaya, Gao, Jorge Orpinel, David  
 611 de la Iglesia Castro, Fábio Santos, Aman Sharma, Dave Berenbaum, Zhanibek, Dani Hodovic,  
 612 daniele, Nikita Kodenko, Andrew Grigorev, Earl, Nabanita Dash, George Vyshnya, Ronan Lamy,  
 613 mayulkarni, Max Hora, Vera, and Sanidhya Mangal. Dvc: Data version control - git for data &  
 614 models, 2022. URL <https://doi.org/10.5281/zenodo.7083378>.

615 Henry Kvinge, Grayson Jorgenson, Davis Brown, Charles Godfrey, and Tegan Emerson. Internal  
 616 representations of vision models through the lens of frames on data manifolds. In *NeurIPS 2023*  
 617 *Workshop on Symmetry and Geometry in Neural Representations*, 2022.

618 Zorah Lähner and Michael Moeller. On the direct alignment of latent spaces. In Marco Fumero,  
 619 Emanuele Rodolà, Clementine Domine, Francesco Locatello, Karolina Dziugaite, and Caron  
 620 Mathilde (eds.), *Proceedings of UniReps: the First Workshop on Unifying Representations in*  
 621 *Neural Models*, volume 243 of *Proceedings of Machine Learning Research*, pp. 158–169. PMLR,  
 622 15 Dec 2024. URL <https://proceedings.mlr.press/v243/lahner24a.html>.

623 Yanyu Li, Geng Yuan, Yang Wen, Ju Hu, Georgios Evangelidis, Sergey Tulyakov, Yanzhi Wang,  
 624 and Jian Ren. EfficientFormer: Vision transformers at MobileNet speed. In *Advances in Neural*  
 625 *Information Processing Systems*, 2022.

626 Zhu Liao, Victor Quétu, Van-Tam Nguyen, and Enzo Tartaglione. Can unstructured pruning reduce  
 627 the depth in deep neural networks? In *Proceedings of the IEEE/CVF International Conference on*  
 628 *Computer Vision*, pp. 1402–1406, 2023.

629 Xinyin Ma, Gongfan Fang, and Xinchao Wang. Llm-pruner: On the structural pruning of large  
 630 language models. *Advances in neural information processing systems*, 36:21702–21720, 2023.

631 Valentino Maiorca, Luca Moschella, Antonio Norelli, Marco Fumero, Francesco Locatello, and  
 632 Emanuele Rodolà. Latent space translation via semantic alignment. *Advances in Neural Information*  
 633 *Processing Systems*, 36, 2024.

634 Ari Morcos, Maithra Raghu, and Samy Bengio. Insights on representational similarity in neural  
 635 networks with canonical correlation. *Advances in Neural Information Processing Systems*, 31,  
 636 2018.

637 Luca Moschella, Valentino Maiorca, Marco Fumero, Antonio Norelli, Francesco Locatello, and  
 638 Emanuele Rodolà. Relative representations enable zero-shot latent space communication. In *Proc.*  
 639 *ICLR*, 2023.

640 Thao Nguyen, Maithra Raghu, and Simon Kornblith. Do wide and deep networks learn the same  
 641 things? uncovering how neural network representations vary with width and depth. *arXiv preprint*  
 642 *arXiv:2010.15327*, 2020.

648 Antonio Norelli, Marco Fumero, Valentino Maiorca, Luca Moschella, Emanuele Rodola, and  
 649 Francesco Locatello. Asif: Coupled data turns unimodal models to multimodal without training.  
 650 *Advances in Neural Information Processing Systems*, 36:15303–15319, 2023.

651

652 Maxime Oquab, Timothée Darcet, Théo Moutakanni, Huy Vo, Marc Szafraniec, Vasil Khalidov,  
 653 Pierre Fernandez, Daniel Haziza, Francisco Massa, Alaaeldin El-Nouby, et al. Dinov2: Learning  
 654 robust visual features without supervision. *arXiv preprint arXiv:2304.07193*, 2023.

655

656 Junting Pan, Adrian Bulat, Fuwen Tan, Xiatian Zhu, Lukasz Dudziak, Hongsheng Li, Georgios  
 657 Tzimiropoulos, and Brais Martinez. EdgeViTs: Competing light-weight CNNs on mobile devices  
 658 with vision transformers. In *European Conference on Computer Vision (ECCV)*, 2022.

659

660 Alec Radford, Jong Wook Kim, Chris Hallacy, Aditya Ramesh, Gabriel Goh, Sandhini Agarwal,  
 661 Girish Sastry, Amanda Askell, Pamela Mishkin, Jack Clark, et al. Learning transferable visual  
 662 models from natural language supervision. In *International conference on machine learning*, pp.  
 663 8748–8763. PMLR, 2021.

664

665 Maithra Raghu, Justin Gilmer, Jason Yosinski, and Jascha Sohl-Dickstein. Svcca: Singular vector  
 666 canonical correlation analysis for deep learning dynamics and interpretability. *Advances in neural  
 667 information processing systems*, 30, 2017.

668

669 Olga Russakovsky, Jia Deng, Hao Su, Jonathan Krause, Sanjeev Satheesh, Sean Ma, Zhiheng Huang,  
 670 Andrej Karpathy, Aditya Khosla, Michael Bernstein, Alexander C. Berg, and Li Fei-Fei. ImageNet  
 671 Large Scale Visual Recognition Challenge. *International Journal of Computer Vision (IJCV)*, 115  
 672 (3):211–252, 2015. doi: 10.1007/s11263-015-0816-y.

673

674 Hassan Sajjad, Fahim Dalvi, Nadir Durrani, and Preslav Nakov. On the effect of dropping layers of  
 675 pre-trained transformer models. *Computer Speech & Language*, 77:101429, 2023.

676

677 Christoph Schuhmann, Romain Beaumont, Richard Vencu, Cade Gordon, Ross Wightman, Mehdi  
 678 Cherti, Theo Coombes, Aarush Katta, Clayton Mullis, Mitchell Wortsman, Patrick Schramowski,  
 679 Srivatsa Kundurthy, Katherine Crowson, Ludwig Schmidt, Robert Kaczmarczyk, and Jenia  
 680 Jitsev. Laion-5b: An open large-scale dataset for training next generation image-text models. In  
 681 S. Koyejo, S. Mohamed, A. Agarwal, D. Belgrave, K. Cho, and A. Oh (eds.), *Advances in Neural  
 682 Information Processing Systems*, volume 35, pp. 25278–25294. Curran Associates, Inc., 2022.  
 683 URL [https://proceedings.neurips.cc/paper\\_files/paper/2022/file/a1859debfb3b59d094f3504d5ebb6c25-Paper-Datasets\\_and\\_Benchmarks.pdf](https://proceedings.neurips.cc/paper_files/paper/2022/file/a1859debfb3b59d094f3504d5ebb6c25-Paper-Datasets_and_Benchmarks.pdf).

684

685 Sidak Pal Singh and Dan Alistarh. Woodfisher: Efficient second-order approximation for neural  
 686 network compression. In H. Larochelle, M. Ranzato, R. Hadsell, M.F. Balcan, and H. Lin (eds.),  
 687 *Advances in Neural Information Processing Systems*, volume 33, pp. 18098–18109. Curran Asso-  
 688 ciates, Inc., 2020. URL [https://proceedings.neurips.cc/paper\\_files/paper/2020/file/d1ff1ec86b62cd5f3903ff19c3a326b2-Paper.pdf](https://proceedings.neurips.cc/paper_files/paper/2020/file/d1ff1ec86b62cd5f3903ff19c3a326b2-Paper.pdf).

689

690 Mingjie Sun, Zhuang Liu, Anna Bair, and J Zico Kolter. A simple and effective pruning approach for  
 691 large language models. *arXiv preprint arXiv:2306.11695*, 2023.

692

693 Shengkun Tang, Yaqing Wang, Zhenglun Kong, Tianchi Zhang, Yao Li, Caiwen Ding, Yanzhi Wang,  
 694 Yi Liang, and Dongkuan Xu. You need multiple exiting: Dynamic early exiting for accelerating  
 695 unified vision language model. In *Proceedings of the IEEE/CVF Conference on Computer Vision  
 696 and Pattern Recognition*, pp. 10781–10791, 2023.

697

698 Hugo Touvron, Matthieu Cord, Matthijs Douze, Francisco Massa, Alexandre Sablayrolles, and Hervé  
 699 Jegou. Training data-efficient image transformers & distillation through attention. arxiv 2020.  
 700 *arXiv preprint arXiv:2012.12877*, 2(3), 2020.

701

702 Hugo Touvron, Matthieu Cord, Matthijs Douze, Francisco Massa, Alexandre Sablayrolles, and Hervé  
 703 Jegou. Training data-efficient image transformers & distillation through attention. In Marina Meila  
 704 and Tong Zhang (eds.), *Proceedings of the 38th International Conference on Machine Learning*,  
 705 volume 139 of *Proceedings of Machine Learning Research*, pp. 10347–10357. PMLR, 18–24 Jul  
 706 2021. URL <https://proceedings.mlr.press/v139/touvron21a.html>.

702 Lucrezia Valeriani, Diego Doimo, Francesca Cutrello, Alessandro Laio, Alessio Ansuini, and  
 703 Alberto Cazzaniga. The geometry of hidden representations of large transformer models. *Advances*  
 704 *in Neural Information Processing Systems*, 36, 2024.

705 Andreas Veit and Serge Belongie. Convolutional networks with adaptive inference graphs. In  
 706 *Proceedings of the European Conference on Computer Vision (ECCV)*, September 2018.

707 Andreas Veit, Michael J Wilber, and Serge Belongie. Residual networks behave like ensem-  
 708 bles of relatively shallow networks. In D. Lee, M. Sugiyama, U. Luxburg, I. Guyon, and  
 709 R. Garnett (eds.), *Advances in Neural Information Processing Systems*, volume 29. Curran Asso-  
 710 ciates, Inc., 2016. URL [https://proceedings.neurips.cc/paper\\_files/paper/2016/file/37bc2f75bf1bcfe8450ala41c200364c-Paper.pdf](https://proceedings.neurips.cc/paper_files/paper/2016/file/37bc2f75bf1bcfe8450ala41c200364c-Paper.pdf).

711 Shashanka Venkataramanan, Amir Ghodrati, Yuki M Asano, Fatih Porikli, and Amir Habibian. Skip-  
 712 attention: Improving vision transformers by paying less attention. In *The Twelfth International*  
 713 *Conference on Learning Representations*, 2024. URL <https://openreview.net/forum?id=vI95kcLAoU>.

714 Guo-Hua Wang and Jianxin Wu. Practical network acceleration with tiny sets. In *Proceedings of the*  
 715 *IEEE/CVF Conference on Computer Vision and Pattern Recognition*, 2023.

716 Benjamin Warner, Antoine Chaffin, Benjamin Clavié, Orion Weller, Oskar Hallström, Said  
 717 Taghadouini, Alexis Gallagher, Raja Biswas, Faisal Ladhak, Tom Aarsen, et al. Smarter, better,  
 718 faster, longer: A modern bidirectional encoder for fast, memory efficient, and long context finetun-  
 719 ing and inference. In *Proceedings of the 63rd Annual Meeting of the Association for Computational*  
 720 *Linguistics (Volume 1: Long Papers)*, pp. 2526–2547, 2025.

721 Zuxuan Wu, Tushar Nagarajan, Abhishek Kumar, Steven Rennie, Larry S. Davis, Kristen Grauman,  
 722 and Rogerio Feris. Blockdrop: Dynamic inference paths in residual networks. In *Proceedings of*  
 723 *the IEEE Conference on Computer Vision and Pattern Recognition (CVPR)*, June 2018.

724 Han Xiao, Kashif Rasul, and Roland Vollgraf. Fashion-mnist: a novel image dataset for benchmarking  
 725 machine learning algorithms. *arXiv preprint arXiv:1708.07747*, 2017.

726 Ji Xin, Raphael Tang, Jaejun Lee, Yaoliang Yu, and Jimmy Lin. Deebert: Dynamic early exiting for  
 727 accelerating bert inference. *arXiv preprint arXiv:2004.12993*, 2020.

728 Fang Yu, Kun Huang, Meng Wang, Yuan Cheng, Wei Chu, and Li Cui. Width & depth pruning for  
 729 vision transformers. In *Proc. AAAI*, 2022.

730 Xiaohua Zhai, Joan Puigcerver, Alexander Kolesnikov, Pierre Ruyssen, Carlos Riquelme, Mario  
 731 Lucic, Josip Djolonga, Andre Susano Pinto, Maxim Neumann, Alexey Dosovitskiy, et al. A  
 732 large-scale study of representation learning with the visual task adaptation benchmark. *arXiv*  
 733 *preprint arXiv:1910.04867*, 2019.

734 Hanxiao Zhang, Yifan Zhou, and Guo-Hua Wang. Dense vision transformer compression with few  
 735 samples. In *Proceedings of the IEEE/CVF Conference on Computer Vision and Pattern Recognition*  
 736 (*CVPR*), pp. 15825–15834, June 2024.

737 Minjia Zhang and Yuxiong He. Accelerating training of transformer-based language models with  
 738 progressive layer dropping. *Advances in neural information processing systems*, 33:14011–14023,  
 739 2020.

740 Xiang Zhang, Junbo Jake Zhao, and Yann LeCun. Character-level convolutional networks for text  
 741 classification. In *NIPS*, 2015.

742 Bolei Zhou, Hang Zhao, Xavier Puig, Sanja Fidler, Adela Barriuso, and Antonio Torralba. Semantic  
 743 understanding of scenes through the ade20k dataset. *arXiv preprint arXiv:1608.05442*, 2016.

744 Bolei Zhou, Hang Zhao, Xavier Puig, Sanja Fidler, Adela Barriuso, and Antonio Torralba. Scene  
 745 parsing through ade20k dataset. In *Proceedings of the IEEE Conference on Computer Vision and*  
 746 *Pattern Recognition*, 2017.

747 Wangchunshu Zhou, Canwen Xu, Tao Ge, Julian McAuley, Ke Xu, and Furu Wei. Bert loses patience:  
 748 Fast and robust inference with early exit. *Advances in Neural Information Processing Systems*, 33:  
 749 18330–18341, 2020.

756 A APPENDIX  
757758 A.1 IMPLEMENTATION DETAILS  
759760 This section details the experiments conducted in Section 4, providing information to reproduce them.  
761 Additionally, we provide the code as a zip file in the supplementary material.  
762763 A.1.1 MODELS AND DATASETS  
764765 Table 7 contains the full list of the pretrained models, while Table 8 contains dataset information.  
766767 Table 7: **Pretrained models details.** Details of the pretrained feature extractors with their Hugging-  
768 Face key, their alias, and their latent space dimensionality.  
769

Modality	HuggingFace Model Name	Alias	Enc. Dim
Vision	WinKawaks/vit-tiny-patch16-224	ViT-T (Dosovitskiy et al., 2021)	192
	WinKawaks/vit-small-patch16-224	ViT-S (Dosovitskiy et al., 2021)	384
	facebook/dinov2-small	DiNO-S (Oquab et al., 2023)	384
	facebook/deit-small-patch16-224	DEiT-S (Touvron et al., 2020)	384
	google/vit-base-patch16-224	ViT-B (Dosovitskiy et al., 2021)	768
	facebook/dinov2-base	DiNO-B (Oquab et al., 2023)	768
Text	laion/CLIP-ViT-B-16-laion2B-s34B-b88K	OpenCLIP-ViT-B (Zhai et al., 2019)	768
	google/vit-large-patch16-224	ViT-L (Dosovitskiy et al., 2021)	1024
Text	answerdotai/ModernBERT-base	ModernBERT-B (Warner et al., 2025)	768

781 Table 8: **Dataset details.** Details of the HuggingFace datasets used in the classification and recon-  
782 struction experiments, with the associated number of classes.  
783

Modality	Name	Alias	# Classes
Vision	MNIST (Deng, 2012)	MNIST	10
	Fashion-MNIST (Xiao et al., 2017)	F-MNIST	10
	CIFAR-10 (Krizhevsky et al., 2009)	CIFAR-10	10
	CIFAR-100 (coarse) (Krizhevsky et al., 2009)	CIFAR-100C	20
	CIFAR-100 (fine) (Krizhevsky et al., 2009)	CIFAR-100F	100
	SceneParse150 (Zhou et al., 2017; 2016)	SceneParse150	150
Text	Imagenet-1k (Russakovsky et al., 2015)	ImageNet1k	1000
	AG News Zhang et al. (2015)	AG News	4

795 A.1.2 APPROXIMATORS  
796797 The first implementation, referred to as the Res-MLP, is composed of two normalization layers and  
798 a feedforward submodule. The first layer normalization processes the input tensor, followed by a  
799 feedforward submodule comprising a linear transformation, a SiLU activation, a dropout layer, and  
800 a final linear transformation. The output of the feedforward submodule is added to the normalized  
801 input via a residual connection. This sum is then passed through the second normalization layer  
802 to produce the final output. The second implementation, referred to as the MLP, is a simplified  
803 MLP that employs a sequential architecture with a first linear transformation that reduces the input  
804 dimensionality to half of the target dimension, followed by a GELU activation function for smooth  
805 non-linearity, and a final linear transformation that restores the reduced features to match the target  
806 dimensionality. Refer to Listings 1 and 2 for the code snippet of the two translators.  
807808 Listing 1: Python Code Snippet for the Res-MLP translator  
809

```
class ResMLP(nn.Module):
    def __init__(self, num_features: int, dropout_p: float):
```

```
810     super().__init__()
811
812     self.norm1 = nn.LayerNorm(num_features)
813     self.norm2 = nn.LayerNorm(num_features)
814
815     self.ff = nn.Sequential(
816         nn.Linear(num_features, num_features),
817         nn.SiLU(),
818         nn.Dropout(p=dropout_p),
819         nn.Linear(num_features, num_features),
820     )
821
822     def forward(self, x: torch.Tensor) -> torch.Tensor:
823         x_normalized = self.norm1(x)
824         x_transformed = self.ff(x_normalized)
825         return self.norm2(x_transformed + x_normalized)
```

Listing 2: Python Code Snippet for the MLP translator

```
826     translation = nn.Sequential(  
827         nn.Linear(x.size(1), y.size(1) // 2),  
828         nn.GELU(),  
829         nn.Linear(y.size(1) // 2, y.size(1)),  
830     )
```

### A.1.3 METRIC ABLATION

We introduce linear approximation error as a simple, stable, and sample-efficient criterion for identifying redundant transformer blocks, offering a practical alternative for guiding block approximation. This metric measures how well the representation of a later block can be reconstructed from an earlier one through a least-squares projection, providing a direct estimate of how much additional structure the skipped layers contribute. Importantly, the error can be estimated using as few as 50 samples producing substantially more stable and interpretable rankings compared to other metrics.

Table 9: **Top-5 Block Approximation Recommendation.** Top 5 recommended blocks to be approximated based on linear approximation error using DEiT-S and CIFAR-100F.

Rank	Approx	# Layers	Predicted Error	Accuracy %
1	$9 \rightarrow 10$	1	0.14	$71.69 \pm 0.11$
2	$10 \rightarrow 11$	1	0.18	$71.17 \pm 0.19$
3	$8 \rightarrow 9$	1	0.23	$70.83 \pm 0.13$
4	$9 \rightarrow 11$	2	0.25	$71.14 \pm 0.15$
5	$8 \rightarrow 10$	2	0.26	$71.06 \pm 0.19$
-	original	0	-	71.1

As shown in Table 9, linear approximation error correlates strongly with the actual accuracy impact of skipping or approximating a block range: blocks with the lowest error consistently incur minimal or no downstream performance degradation. This makes the metric both computationally lightweight and practically reliable for identifying redundant or compressible transformer regions.

To further validate this choice, we conduct an ablation comparing several candidate similarity metrics (e.g., cosine distance, MSE, Euclidean distance, and CKA) and evaluate how well each predicts the true accuracy drop after approximation. Results, summarized in Table 10, show that linear approximation error achieves the most consistent performance across architectures, with competitive or superior Precision@5 and Recall@5 scores. Notably, metrics such as cosine distance and Euclidean distance exhibit behavior that is highly model-dependent, while CKA performs well in some cases but is less stable across architectures and budgets.

Overall, this ablation highlights that linear approximation error provides the best trade-off between stability, computational cost, and predictive fidelity, making it a strong default metric for block selection in transformer approximation.

864  
 865 Table 10: **Block Selection Strategy Ablation.** Ranking evaluation metrics for approximation quality  
 866 prediction on CIFAR-100 using DEiT-S, DiNO-S, and DiNO-B. Precision@5 and Recall@5 are  
 867 shown for each model.

	DEiT-S		DiNO-S		DiNO-B		Mean	
	P@5	R@5	P@5	R@5	P@5	R@5	P@5	R@5
Linear Error	0.6	0.6	0.6	0.6	0.6	0.6	0.60	0.60
Cosine	1.0	1.0	0.4	0.4	0.2	0.2	0.53	0.53
CKA	0.6	0.6	0.6	0.6	0.4	0.4	0.53	0.53
MSE	0.0	0.0	0.4	0.4	0.6	0.6	0.33	0.33
Euclidean	0.8	0.8	0.4	0.4	0.4	0.4	0.53	0.53

#### 875 876 A.1.4 BLOCK SELECTION PSEUDOCODE

---

##### 879 **Algorithm 1** Identify Top- $k$ Layer Skip Configurations

880 **Require:** Model encoder  $\mathcal{M}$  with  $L$  layers, dataset  $\mathcal{D}$ , number of top configurations  $k$ , skip budget  $b$   
 881 (optional)  
 882 **Ensure:** Top- $k$  skip configurations  $\mathcal{S} = \{(s_1, e_1), \dots, (s_k, e_k)\}$   
 883 1: Extract layer representations:  $\mathbf{H}_i \leftarrow \text{encode}(\mathcal{M}, \mathcal{D}, \text{layer}_i)$  for  $i \in [0, L]$   
 884 2: Initialize error matrix  $\mathbf{E} \in \mathbb{R}^{L \times L}$   
 885 3: **for**  $i = 0$  to  $L - 1$  **do**  
 886   4:   **for**  $j = i + 1$  to  $L$  **do**  
 887     5:      $\mathbf{E}_{i,j} \leftarrow \text{LinearApproximationError}(\mathbf{H}_i, \mathbf{H}_j)$   
 888   6:   **end for**  
 889   7: **end for**  
 890 8: Initialize candidate list  $\mathcal{C} \leftarrow \emptyset$   
 891 9: **for**  $i = 0$  to  $L - 1$  **do**  
 892   10:   **for**  $j = i + 1$  to  $L$  **do**  
 893     11:     **if**  $b$  is specified and  $j - i \neq b$  **then**  
 894       12:       **continue** ▷ Skip if not matching budget  
 895     13:     **end if**  
 896     14:      $\mathcal{C} \leftarrow \mathcal{C} \cup \{(i, j, \mathbf{E}_{i,j})\}$   
 897   15: **end for**  
 898 16: **end for**  
 899 17: Sort  $\mathcal{C}$  by error in ascending order  
 900 18:  $\mathcal{S} \leftarrow$  top- $k$  configurations from  $\mathcal{C}$   
 901 19: **return**  $\mathcal{S}$

---

##### 902 **Algorithm 2** Linear Approximation Error

903 **Require:** Source layer representations  $\mathbf{X} \in \mathbb{R}^{n \times d}$ , target layer representations  $\mathbf{Y} \in \mathbb{R}^{n \times d}$   
 904 **Ensure:** Normalized residual error  $\epsilon$   
 905 1: Solve least-squares:  $\mathbf{W}^* = \arg \min_{\mathbf{W}} \|\mathbf{Y} - \mathbf{X}\mathbf{W}\|_F^2$   
 906 2: Compute prediction:  $\hat{\mathbf{Y}} = \mathbf{X}\mathbf{W}^*$   
 907 3: Compute normalized error:  $\epsilon = \frac{\|\mathbf{Y} - \hat{\mathbf{Y}}\|_F}{\|\mathbf{Y}\|_F}$   
 908 4: **return**  $\epsilon$

---

#### 911 A.1.5 TOOLS & TECHNOLOGIES

912 All the experiments presented in this work employ the following tools:

913  
 914   • *PyTorch Lightning*, to ensure reproducible results while also getting a clean and modular  
 915     codebase;  
 916   • *NN-Template GrokAI (2021)*, to easily bootstrap the project and enforce best practices;

918  
 919 **Table 11: Top-3 Block Approximation Recommendation.** Top 3 recommended blocks to be  
 920 approximated based on linear approximation error and number of blocks to skip using DEiT-S and  
 921 CIFAR-100F.

# Blocks	Rank	Approx.	Predicted Error	Accuracy %
1	1	9 → 10	0.14	71.69 ± 0.11
	2	10 → 11	0.18	71.17 ± 0.19
	3	8 → 9	0.23	70.83 ± 0.13
2	1	9 → 11	0.25	71.14 ± 0.15
	2	8 → 10	0.26	71.06 ± 0.19
	3	7 → 9	0.36	69.00 ± 0.43
3	1	8 → 11	0.36	68.22 ± 0.40
	2	7 → 10	0.38	69.08 ± 0.24
	3	6 → 9	0.45	65.64 ± 0.03
0	-	original	-	71.1

932  
 933  
 934

- *Transformers by HuggingFace*, to get ready-to-use transformers for both text and images;
- *Datasets by HuggingFace*, to access most of the datasets;
- *DVC* (Kuprieiev et al., 2022), for data versioning;
- *fvcore analysis library* (), for calculating GFLOPs;

935 **A.1.6 COMPUTATIONAL RESOURCES**

936 Experiments involving larger models, specifically DiNO-B, OpenCLIP-ViT-B, and ViT-L, were  
 937 conducted on an NVIDIA H100 GPU equipped with 93 GB of memory. All the other experiments  
 938 utilized an NVIDIA GeForce RTX 5090 GPU with 31 GB of memory.

939 **A.1.7 EFFICIENCY METRICS**

940 We evaluated model efficiency using two primary metrics. GFLOPs were used to measure the  
 941 hardware-independent theoretical complexity of a single forward pass, calculated using the *fvcore*  
 942 analysis library. Throughput, measured in samples per second, was used to quantify the practical,  
 943 hardware-dependent inference speed. This was benchmarked by averaging the wall-clock time over  
 944 numerous iterations on a single NVIDIA H100 GPU with a consistent batch size of 256.

945 **A.2 ADDITIONAL EXPERIMENTS**

946 This section presents supplementary experiments to extend those detailed in Section 4.

947 **A.2.1 LATENT ANALYSIS**

948 This section extend the analysis conducted in Section 4.1, to analyze block-wise internal similarities, to  
 949 additional models of different dimensionality: ViT-T, ViT-S, ViT-B and DiNO-S. Additionally,  
 950 we provide visualization using PCA for DiNO-S, DEiT-S, ViT-S, with different datasets and  
 951 approximating both early and late blocks (see Figures 7 to 11).

952  
 953  
 954  
 955  
 956  
 957  
 958  
 959  
 960  
 961  
 962  
 963  
 964  
 965  
 966  
 967  
 968  
 969  
 970  
 971

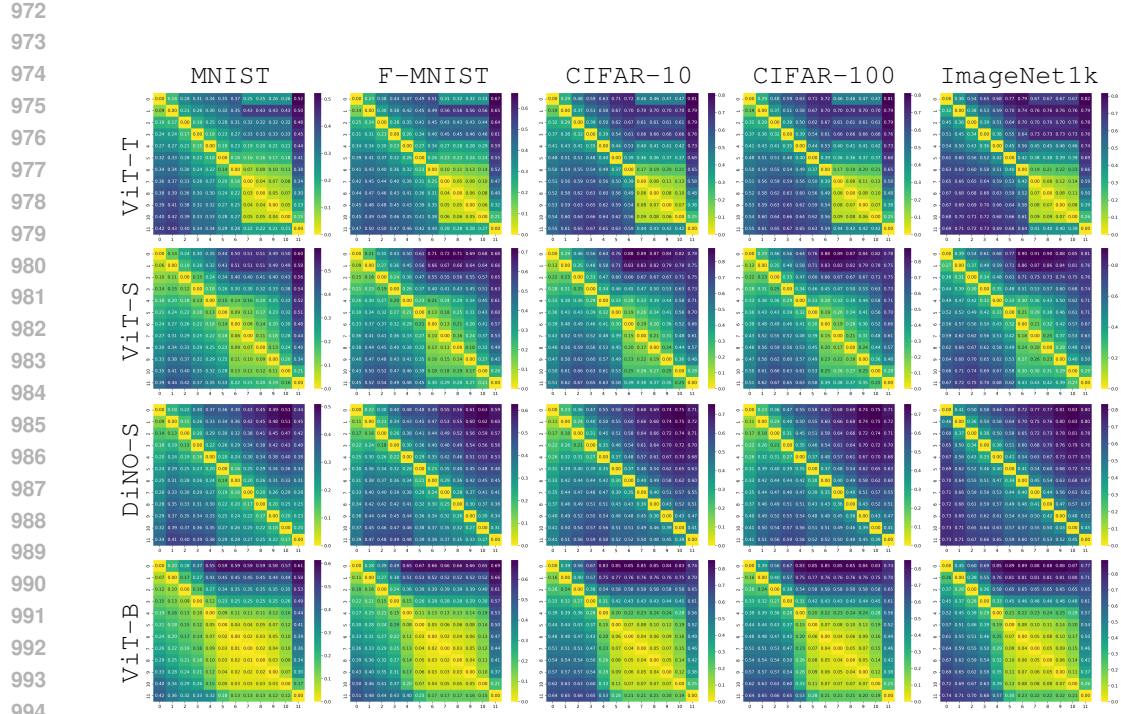


Figure 6: **Block Similarities:** Block-by-block similarities in ViT-T, ViT-S, DiNo-S and ViT-B models across five datasets: MNIST, F-MNIST, CIFAR-10, CIFAR-100 and ImageNet1k. Each matrix quantifies the linear error between latent representations of different blocks, showing potential blocks for approximation. The matrices reveal that the similarity between blocks is predominantly influenced by the model rather than the specific dataset.

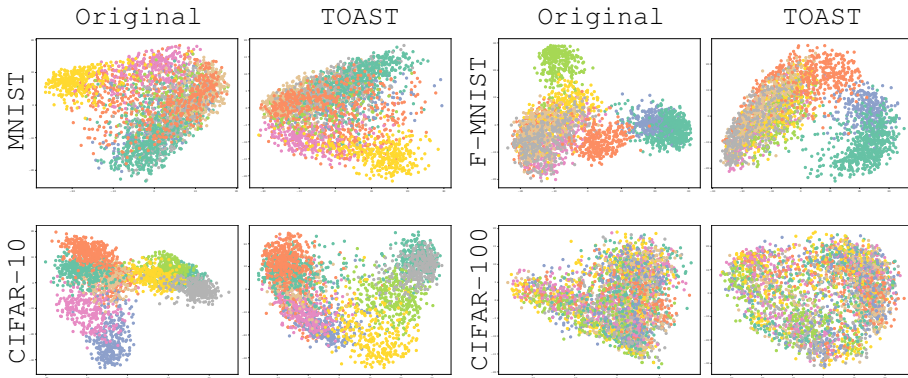
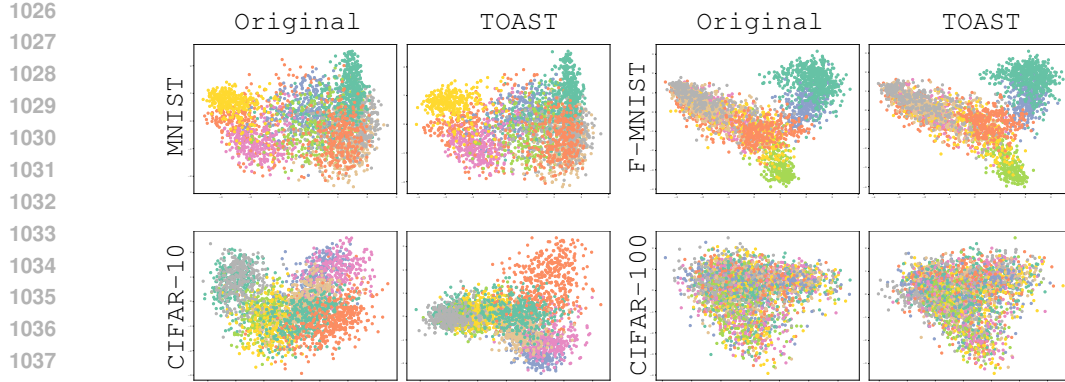
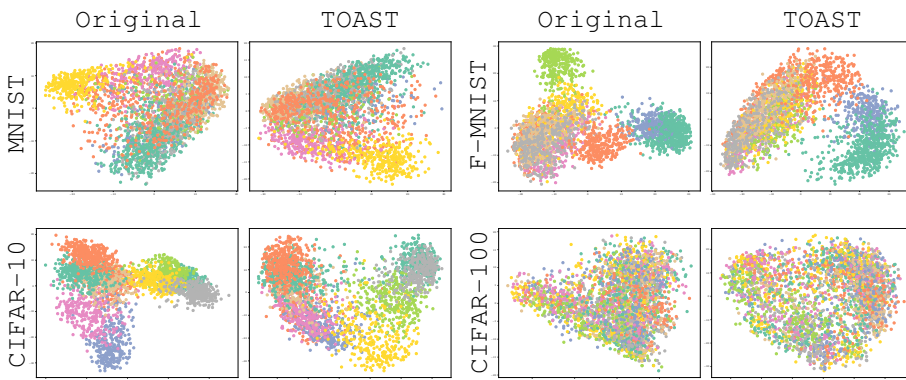


Figure 7: **Last Block Approximation.** PCA visualization of the final layer representations for both the original model and the model with its last block approximated from the preceding one. The representations are generated using the DiNo-S model across four datasets. The plots highlight that the last layer representations in this model are crucial, making it more effective to approximate earlier blocks instead. Note that for CIFAR-100 (bottom right), only the overall structure of the space can be observed, as the 100 classes make it challenging to distinguish labels based on color.



1039  
1040  
1041  
1042  
1043  
1044  
1045  
1046  
1047  
1048  
1049  
1050  
1051  
1052  
1053  
1054  
1055  
1056  
1057  
1058

**Figure 8: Last Block Approximation.** PCA visualization of the final layer representations for both the original model and the model with its last block approximated by the preceding one. The representations are generated using the DEiT-S model across four datasets. The plots highlight that in this model, the representations in the last layer are redundant and can be effectively approximated, offering potential performance improvements while reducing model complexity and parameter count. Note that for CIFAR-100 (bottom right), only the overall structure of the space can be observed, as the 100 classes make it challenging to distinguish labels based on color.



1064  
1065  
1066  
1067  
1068  
1069  
1070  
1071  
1072  
1073  
1074  
1075  
1076  
1077  
1078  
1079

**Figure 9: Last Block Approximation.** PCA visualization of the final layer representations for both the original model and the model with its second block approximated by the preceding one. The representations are generated using the DiNo-S model across four datasets. Note that for CIFAR-100 (bottom right), only the overall structure of the space can be observed, as the 100 classes make it challenging to distinguish labels based on color.

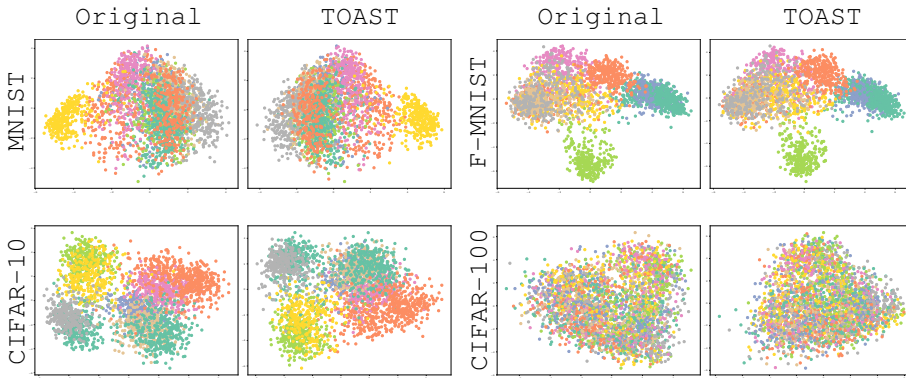


**Figure 10: Last Block Approximation.** PCA visualization of the last layer representations for both the original model and the model with its second block approximated using the previous one. Representations refer to the using ViT-S model across four datasets.

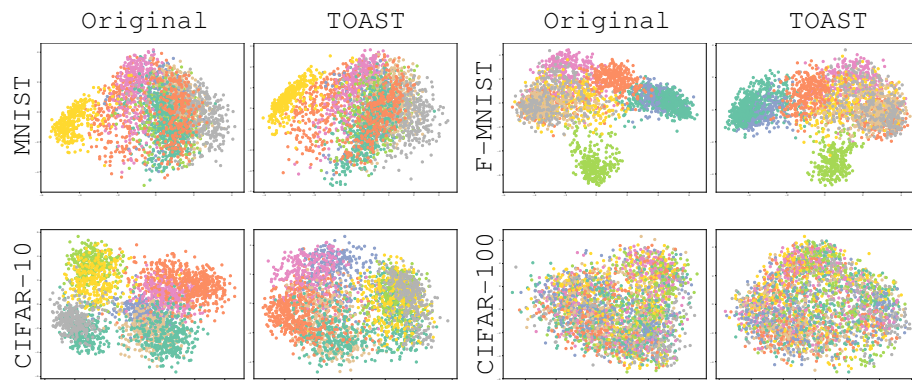


Figure 11: **Last Block Approximation.** PCA visualization of the last layer representations for both the original model and the model with its last block approximated from the previous one. Representations refer to the using ViT-S model across four datasets.

1134  
1135 A.2.2 IMAGE CLASSIFICATION1136 This section presents additional experiments that complement and extend those detailed in Section 4.2.  
1137 Datasets and models are the ones detailed in Tables 7 and 8.1138  
1139 Table 12: **ViT-S Image Classification Performance Across Seeds.** Classification accuracy scores  
1140 for ViT-S using multiple datasets, and 3 seeds. The “Approx.” column specifies the blocks used for  
1141 approximation, where the first value represents the block whose output is used to approximate the  
1142 second block’s output, while the “Params.” column shows the number of parameters removed by the  
1143 approximation compared to the original model.

Approx.	Params.	MNIST	F-MNIST	CIFAR-10	CIFAR-100C	CIFAR-100F	ImageNet1k
1 → 5	15.31M	92.28 ± 0.81	86.90 ± 0.72	85.07 ± 0.55	68.01 ± 0.31	59.21 ± 0.12	44.04 ± 0.42
2 → 5	16.94M	94.76 ± 0.20	88.57 ± 0.31	91.01 ± 0.37	77.77 ± 0.22	69.75 ± 0.36	60.38 ± 0.12
7 → 10	16.94M	94.58 ± 0.28	88.44 ± 0.35	87.36 ± 0.17	72.58 ± 0.69	62.03 ± 0.56	35.80 ± 0.11
1 → 3	18.56M	94.60 ± 0.78	88.36 ± 0.44	91.97 ± 0.16	79.36 ± 0.54	72.41 ± 0.08	64.99 ± 0.29
2 → 4	18.56M	95.08 ± 0.18	88.83 ± 0.21	92.86 ± 0.11	81.45 ± 0.44	74.43 ± 0.27	67.52 ± 0.16
3 → 5	18.56M	94.75 ± 0.57	88.81 ± 0.19	94.09 ± 0.06	83.16 ± 0.34	76.17 ± 0.45	67.27 ± 0.45
1 → 2, 3 → 4	18.56M	94.68 ± 0.69	88.30 ± 0.25	91.91 ± 0.25	79.72 ± 0.16	72.17 ± 0.15	65.38 ± 0.03
1 → 2, 4 → 5	18.56M	94.58 ± 0.77	88.95 ± 0.07	92.29 ± 0.28	80.14 ± 0.10	72.45 ± 0.35	64.42 ± 0.24
0 → 1	20.43M	<b>95.69</b> ± 0.29	88.81 ± 0.19	93.68 ± 0.22	83.55 ± 0.23	76.49 ± 0.29	65.11 ± 0.27
1 → 2	20.43M	95.40 ± 0.57	88.53 ± 0.63	93.90 ± 0.11	83.98 ± 0.22	76.99 ± 0.26	70.32 ± 0.38
2 → 3	20.43M	95.43 ± 0.45	88.93 ± 0.62	94.90 ± 0.26	85.72 ± 0.48	78.96 ± 0.05	71.26 ± 0.03
3 → 4	20.43M	95.43 ± 0.39	88.77 ± 0.36	95.05 ± 0.17	85.99 ± 0.37	79.49 ± 0.32	<b>71.40</b> ± 0.22
4 → 5	20.43M	95.39 ± 0.35	89.18 ± 0.51	<b>95.41</b> ± 0.12	86.27 ± 0.27	<b>79.61</b> ± 0.14	70.98 ± 0.16
5 → 6	20.43M	95.14 ± 0.56	89.30 ± 0.54	94.89 ± 0.27	<b>86.49</b> ± 0.33	79.29 ± 0.19	69.25 ± 0.09
6 → 7	20.43M	95.11 ± 0.42	88.94 ± 0.66	94.81 ± 0.26	85.33 ± 0.30	78.06 ± 0.17	67.41 ± 0.08
7 → 8	20.43M	95.64 ± 0.46	89.41 ± 0.45	94.50 ± 0.34	85.30 ± 0.50	78.03 ± 0.12	66.22 ± 0.10
8 → 9	20.43M	95.36 ± 0.47	<b>89.64</b> ± 0.37	94.36 ± 0.14	84.66 ± 0.25	77.88 ± 0.20	64.03 ± 0.29
9 → 10	20.43M	95.52 ± 0.41	89.57 ± 0.10	94.58 ± 0.27	81.76 ± 0.34	76.45 ± 0.22	61.82 ± 0.24
10 → 11	20.43M	94.83 ± 0.20	89.11 ± 0.43	94.08 ± 0.27	82.13 ± 0.70	77.45 ± 0.29	63.92 ± 0.25
original	22.06M	<u>95.59</u> ± 0.42	<u>89.04</u> ± 0.85	<u>95.68</u> ± 0.24	<u>87.61</u> ± 0.39	<u>81.50</u> ± 0.39	<u>73.24</u> ± 0.13

1160  
1161 Table 13: **DiNO-S Image Classification Performance Across Seeds.** Classification accuracy scores  
1162 for DiNO-S using multiple datasets, and 3 seeds. The “Approx.” column specifies the blocks used  
1163 for approximation, where the first value represents the block whose output is used to approximate the  
1164 second block’s output, while the “Params.” column shows the number of parameters removed by the  
1165 approximation compared to the original model.

Approx.	Params.	MNIST	F-MNIST	CIFAR-10	CIFAR-100C	CIFAR-100F	ImageNet1k
1 → 5	15.31M	96.25 ± 0.30	86.50 ± 1.42	80.11 ± 0.95	59.15 ± 0.45	51.24 ± 0.51	18.70 ± 0.09
2 → 5	16.94M	95.86 ± 0.52	87.99 ± 0.30	85.28 ± 0.99	67.50 ± 1.02	59.57 ± 0.45	40.63 ± 0.59
7 → 10	16.94M	96.05 ± 1.44	88.28 ± 1.25	91.00 ± 0.82	78.47 ± 0.61	70.56 ± 0.25	45.66 ± 0.69
1 → 3	18.56M	96.61 ± 0.34	88.48 ± 0.61	91.73 ± 0.36	78.62 ± 0.87	72.33 ± 0.37	56.85 ± 0.21
2 → 4	18.56M	96.79 ± 0.58	88.34 ± 0.33	91.31 ± 0.16	76.41 ± 0.44	69.71 ± 0.31	60.16 ± 0.41
3 → 5	18.56M	96.76 ± 1.02	88.65 ± 0.92	91.00 ± 0.49	75.51 ± 0.45	69.31 ± 0.05	57.47 ± 0.11
1 → 2, 3 → 4	18.56M	96.71 ± 0.62	88.69 ± 0.46	92.57 ± 0.54	79.16 ± 1.02	72.88 ± 0.57	59.79 ± 0.19
1 → 2, 4 → 5	18.56M	96.81 ± 0.31	88.67 ± 1.23	93.50 ± 0.26	79.35 ± 1.00	73.55 ± 0.38	58.62 ± 0.25
0 → 1	20.43M	96.71 ± 0.79	88.97 ± 1.12	<b>95.67</b> ± 0.12	<b>85.89</b> ± 0.56	<b>80.15</b> ± 0.35	61.25 ± 0.22
1 → 2	20.43M	96.69 ± 0.90	88.26 ± 1.10	95.38 ± 0.09	84.86 ± 0.84	79.38 ± 0.23	64.86 ± 0.36
2 → 3	20.43M	96.42 ± 0.36	88.31 ± 1.20	94.71 ± 0.33	84.15 ± 0.94	77.74 ± 0.85	65.16 ± 0.69
3 → 4	20.43M	96.82 ± 0.68	88.77 ± 0.78	94.87 ± 0.30	83.96 ± 0.62	77.71 ± 0.08	<b>65.35</b> ± 0.56
4 → 5	20.43M	96.82 ± 0.60	89.15 ± 0.72	94.63 ± 0.26	83.04 ± 0.62	77.13 ± 0.17	64.28 ± 0.24
5 → 6	20.43M	96.81 ± 0.85	88.75 ± 0.86	95.33 ± 0.19	84.83 ± 0.04	79.37 ± 0.25	64.88 ± 0.43
6 → 7	20.43M	<b>96.99</b> ± 0.88	<b>89.42</b> ± 0.68	95.21 ± 0.10	83.82 ± 0.53	78.54 ± 0.64	63.61 ± 0.62
7 → 8	20.43M	96.76 ± 0.38	89.05 ± 1.29	95.37 ± 0.14	84.57 ± 0.42	78.95 ± 0.37	61.59 ± 0.31
8 → 9	20.43M	96.62 ± 0.85	88.45 ± 1.21	95.21 ± 0.36	84.98 ± 0.22	79.35 ± 0.22	61.73 ± 0.43
9 → 10	20.43M	96.66 ± 0.33	88.53 ± 0.71	94.55 ± 0.25	83.97 ± 1.25	77.06 ± 0.36	58.56 ± 0.25
10 → 11	20.43M	94.61 ± 0.66	86.96 ± 1.18	92.11 ± 0.32	79.85 ± 0.26	73.01 ± 0.51	50.76 ± 0.33
original	22.06M	<u>96.57</u> ± 0.64	<u>88.07</u> ± 1.40	<u>96.24</u> ± 0.08	<u>87.53</u> ± 0.45	<u>82.04</u> ± 0.42	<u>67.45</u> ± 0.45

1182  
1183  
1184  
1185  
1186  
1187

1188

1189

1190

1191

1192 **Table 14: ViT-T Image Classification Performance.** Classification accuracy scores for ViT-T using  
 1193 multiple datasets, and 3 seeds. The “Approx.” column specifies the blocks used for approximation,  
 1194 where the first value represents the block whose output is used to approximate the second block’s  
 1195 output, while the “Params.” column shows the number of parameters removed by the approximation  
 1196 compared to the original model.

Approx.	Params.	MNIST	F-MNIST	CIFAR-10	CIFAR-100C	CIFAR-100F	ImageNet1k
1 → 5	15.31M	87.66 ± 0.57	85.10 ± 0.42	73.68 ± 0.46	53.46 ± 0.29	44.61 ± 0.42	22.21 ± 0.39
2 → 5	16.94M	90.59 ± 0.79	85.84 ± 0.18	82.41 ± 0.11	62.87 ± 0.21	54.68 ± 0.21	35.14 ± 0.38
7 → 10	16.94M	92.41 ± 0.47	86.50 ± 0.19	82.48 ± 0.85	69.26 ± 0.65	61.15 ± 0.28	39.03 ± 0.13
1 → 3	18.56M	90.55 ± 1.04	85.91 ± 0.22	80.48 ± 0.29	63.43 ± 0.25	54.57 ± 0.32	43.68 ± 0.26
2 → 4	18.56M	92.81 ± 0.56	86.58 ± 0.05	86.85 ± 0.17	70.49 ± 0.30	63.53 ± 0.23	49.94 ± 0.27
3 → 5	18.56M	91.84 ± 0.69	86.80 ± 0.04	88.00 ± 0.04	72.67 ± 0.30	65.66 ± 0.14	48.48 ± 0.37
1 → 2, 3 → 4	18.56M	91.94 ± 0.78	86.71 ± 0.20	83.43 ± 0.41	66.92 ± 0.42	60.07 ± 0.48	45.14 ± 0.15
1 → 2, 4 → 5	18.56M	90.86 ± 0.66	86.57 ± 0.24	84.61 ± 0.14	68.07 ± 0.55	60.11 ± 0.61	44.84 ± 0.26
0 → 1	20.43M	91.74 ± 0.48	86.22 ± 0.23	83.32 ± 0.22	68.58 ± 0.41	61.05 ± 0.36	44.12 ± 0.20
1 → 2	20.43M	91.65 ± 0.61	86.26 ± 0.24	85.84 ± 0.08	71.12 ± 0.06	63.85 ± 0.37	54.34 ± 0.44
2 → 3	20.43M	92.89 ± 0.18	86.49 ± 0.06	88.89 ± 0.08	74.90 ± 0.25	68.03 ± 0.37	57.83 ± 0.07
3 → 4	20.43M	93.10 ± 0.43	<b>87.34</b> ± 0.03	89.73 ± 0.37	76.45 ± 0.17	70.04 ± 0.35	57.55 ± 0.14
4 → 5	20.43M	92.43 ± 0.20	87.22 ± 0.10	90.11 ± 0.32	76.40 ± 0.42	69.97 ± 0.37	55.91 ± 0.10
5 → 6	20.43M	<b>93.57</b> ± 0.11	86.80 ± 0.13	90.17 ± 0.27	76.47 ± 0.35	70.69 ± 0.49	55.43 ± 0.38
6 → 7	20.43M	92.13 ± 0.37	86.77 ± 0.02	87.73 ± 0.22	72.35 ± 0.31	66.73 ± 0.45	47.39 ± 0.45
7 → 8	20.43M	93.20 ± 0.06	86.90 ± 0.30	88.58 ± 0.26	75.80 ± 0.29	69.28 ± 0.41	53.48 ± 0.24
8 → 9	20.43M	92.76 ± 0.11	87.18 ± 0.17	89.57 ± 0.33	76.43 ± 0.50	71.07 ± 0.33	56.07 ± 0.77
9 → 10	20.43M	92.39 ± 0.10	86.74 ± 0.18	89.86 ± 0.31	77.34 ± 0.04	71.70 ± 0.37	57.45 ± 0.29
10 → 11	20.43M	90.92 ± 0.48	86.89 ± 0.12	<b>90.98</b> ± 0.21	<b>78.85</b> ± 0.38	<b>72.29</b> ± 0.42	<b>58.94</b> ± 0.22
original	22.06M	93.22 ± 0.18	<b>86.99</b> ± 0.29	91.29 ± 0.06	79.27 ± 0.23	73.45 ± 0.38	63.02 ± 0.22

1213

1214

1215

1216

1217

1218

1219

1220

1221 **Table 15: ViT-B Image Classification Performance.** Classification accuracy scores for ViT-B using  
 1222 multiple datasets, and 3 seeds. The “Approx.” column specifies the blocks used for approximation,  
 1223 where the first value represents the block whose output is used to approximate the second block’s  
 1224 output, while the “Params.” column shows the number of parameters removed by the approximation  
 1225 compared to the original model.

Approx.	Params.	Accuracy ↑				
		MNIST	F-MNIST	CIFAR-10	CIFAR-100C	CIFAR-100F
1 → 5	-25.99M	87.06 ± 0.53	84.33 ± 0.61	73.54 ± 0.57	51.67 ± 1.10	38.98 ± 0.72
2 → 5	-19.49M	94.20 ± 0.21	87.80 ± 0.24	87.10 ± 0.83	71.68 ± 0.50	61.19 ± 0.37
1 → 3	-13M	96.51 ± 0.42	88.72 ± 0.41	93.71 ± 0.13	83.05 ± 0.23	74.74 ± 0.29
3 → 5	-13M	95.59 ± 0.09	88.28 ± 0.20	93.11 ± 0.06	83.50 ± 0.17	74.35 ± 0.47
2 → 4	-13M	96.21 ± 0.33	89.21 ± 0.64	94.59 ± 0.32	85.13 ± 0.24	76.82 ± 0.41
8 → 10	-13M	96.54 ± 0.21	<b>89.72</b> ± 0.52	95.05 ± 0.26	85.78 ± 0.37	79.62 ± 0.14
9 → 11	-13M	95.59 ± 0.52	89.49 ± 0.26	93.22 ± 0.56	82.23 ± 0.44	76.33 ± 0.10
3 → 4	-6.5M	96.86 ± 0.35	89.69 ± 1.09	<b>96.18</b> ± 0.09	<b>89.18</b> ± 0.06	<b>82.50</b> ± 0.17
4 → 5	6.5M	96.55 ± 0.23	89.13 ± 0.50	95.39 ± 0.23	87.43 ± 0.15	80.30 ± 0.16
0 → 1	-6.5M	96.75 ± 0.29	88.97 ± 0.26	93.74 ± 0.15	84.49 ± 0.20	76.54 ± 0.29
1 → 2	-6.5M	96.88 ± 0.01	89.29 ± 0.24	95.63 ± 0.11	87.46 ± 0.20	80.64 ± 0.23
2 → 3	-6.5M	<b>96.91</b> ± 0.17	89.69 ± 0.61	96.00 ± 0.18	88.38 ± 0.13	81.59 ± 0.35
-	86.39M	95.61 ± 0.22	89.64 ± 0.57	96.25 ± 0.17	89.52 ± 0.23	83.41 ± 0.20

1238

1239

1240

1241

1242 A.2.3 ZERO-SHOT IMAGE CLASSIFICATION  
1243

1244 To further assess the effectiveness of our approach, we evaluate TOAST in a zero-  
1245 shot image classification setting. This evaluation utilizes the OpenCLIP-ViT-B  
1246 model (Radford et al., 2021), which was pretrained on LAION-2B Schuhmann  
1247 et al. (2022), with ImageNet1k serving as the downstream evaluation dataset.

1248  
1249 **Table 16: Zero-shot image classification.**  
1250 Accuracy scores for OpenCLIP-ViT-B on  
1251 ImageNet1k. The "Approx." column specifies  
1252 the blocks being approximated, where the  
1253 first value represents the block whose output is  
1254 used to approximate the second block's output.  
1255 The " $\Delta$ " column indicates the change in accuracy.  
1256

Params.	Approx.	Accuracy $\uparrow$	$\Delta$
	0 $\rightarrow$ 1	57.93	-17.41%
	1 $\rightarrow$ 2	64.20	-8.56%
	2 $\rightarrow$ 3	<b>66.35</b>	<b>-5.51%</b>
	3 $\rightarrow$ 4	64.65	-7.90%
	4 $\rightarrow$ 5	64.86	-7.60%
-6.49M	5 $\rightarrow$ 6	58.05	-17.32%
	6 $\rightarrow$ 7	61.56	-12.31%
	7 $\rightarrow$ 8	58.53	-16.64%
	8 $\rightarrow$ 9	52.32	-25.50%
	9 $\rightarrow$ 10	59.21	-15.68%
	10 $\rightarrow$ 11	22.64	-67.75%
149.07M	original	<u>70.21</u>	-

1271 of our knowledge, this work is the first to investigate training-free model size reduction in this  
1272 challenging setting.  
1273

1274 A.2.4 TOAST APPLICABILITY TO OTHER TASKS OR DOMAINS  
1275

1276 This section presents additional experiments that complement and extend those detailed in Section 4.3.  
1277 Datasets and models are the ones detailed in Tables 7 and 8.  
1278  
1279  
1280  
1281  
1282  
1283  
1284  
1285  
1286  
1287  
1288  
1289  
1290  
1291  
1292  
1293  
1294  
1295

1296  
 1297  
 1298  
 1299  
 1300  
 1301  
 1302  
 1303  
 1304  
 1305  
 1306  
 1307  
 1308  
 1309

1310 **Table 17: TOAST Text Classification Performance on AG News.** Text classification accuracy,  
 1311 GFLOPs, and throughput for ModernBERT-B using AG News. The "Approx." column specifies  
 1312 the block mapping (output of the first block is used to approximate the output of the second). MLP is  
 1313 a trained approximators, while Linear is closed-form and training-free. Results are averaged over  
 1314 three seeds.

1315  
 1316  
 1317  
 1318  
 1319  
 1320  
 1321  
 1322  
 1323  
 1324  
 1325  
 1326  
 1327  
 1328  
 1329  
 1330  
 1331  
 1332  
 1333  
 1334  
 1335  
 1336  
 1337  
 1338  
 1339  
 1340  
 1341  
 1342  
 1343  
 1344  
 1345  
 1346  
 1347  
 1348  
 1349

Approx.	Params ↓	Linear			MLP		
		Accuracy% ↑	GFLOPs ↓	img/s ↑	Accuracy% ↑	GFLOPs ↓	img/s ↑
11 → 21	92.82M	0.81 ± 0.05	12.7	2264.0	0.73 ± 0.00	12.68	2216.50
4 → 8, 11 → 14, 18 → 21	92.82M	0.82 ± 0.07	12.7	2220.7	0.73 ± 0.01	12.68	2155.16
4 → 7, 18 → 21	109.68M	0.82 ± 0.07	15.9	1803.9	0.71 ± 0.02	15.85	1771.80
4 → 8	126.54M	0.86 ± 0.02	19.0	1636.0	0.82 ± 0.01	19.03	1632.65
11 → 14	132.16M	0.86 ± 0.02	20.1	1544.3	0.82 ± 0.01	20.08	1540.23
18 → 21	132.16M	0.85 ± 0.02	20.1	1472.8	0.82 ± 0.01	20.08	1467.56
1 → 2	143.40M	0.84 ± 0.01	22.2	1386.0	0.84 ± 0.00	22.20	1385.20
2 → 3	143.40M	0.86 ± 0.00	22.2	1379.8	0.86 ± 0.00	22.20	1388.06
3 → 4	143.40M	0.82 ± 0.01	22.2	1391.6	0.83 ± 0.00	22.20	1392.14
4 → 5	143.40M	0.88 ± 0.00	22.2	1380.3	0.81 ± 0.01	22.20	1384.42
5 → 6	143.40M	0.86 ± 0.02	22.2	1385.0	0.83 ± 0.00	22.20	1392.14
6 → 7	143.40M	0.86 ± 0.02	22.2	1387.8	0.85 ± 0.01	22.20	1387.81
7 → 8	143.40M	0.87 ± 0.01	22.2	1384.8	0.85 ± 0.00	22.20	1365.78
8 → 9	143.40M	0.84 ± 0.01	22.2	1384.4	0.83 ± 0.01	22.20	1383.31
9 → 10	143.40M	0.82 ± 0.08	22.2	1385.3	0.71 ± 0.01	22.20	1385.92
10 → 11	143.40M	0.81 ± 0.08	22.2	1383.2	0.72 ± 0.03	22.20	1381.78
11 → 12	143.40M	0.87 ± 0.02	22.2	1378.8	0.82 ± 0.01	22.20	1394.63
12 → 13	143.40M	0.86 ± 0.02	22.2	1384.5	0.83 ± 0.01	22.20	1390.65
13 → 14	143.40M	0.80 ± 0.06	22.2	1385.2	0.73 ± 0.02	22.20	1385.23
14 → 15	143.40M	0.84 ± 0.04	22.2	1390.0	0.79 ± 0.01	22.20	1387.43
15 → 16	143.40M	0.85 ± 0.02	22.2	1402.7	0.82 ± 0.00	22.20	1381.80
16 → 17	143.40M	0.87 ± 0.01	22.2	1402.8	0.85 ± 0.00	22.20	1387.02
17 → 18	143.40M	0.85 ± 0.02	22.2	1402.3	0.83 ± 0.01	22.20	1389.71
18 → 19	143.40M	0.87 ± 0.01	22.2	1403.5	0.85 ± 0.01	22.20	1393.53
19 → 20	143.40M	0.85 ± 0.02	22.2	1403.9	0.82 ± 0.00	22.20	1390.19
20 → 21	143.40M	0.87 ± 0.02	22.2	1340.2	0.84 ± 0.00	22.20	1332.27
original	149.01M	0.88 ± 0.00	23.25	1337.25	0.88 ± 0.00	23.25	1347.46

1350 A.2.5 EVALUATION WITH ORIGINAL CLASSIFICATION HEADS  
13511352 **Table 18: Comparison of Original vs. Retrained Classification Heads.** TOAST performance on  
1353 ImageNet1k using the frozen, pre-trained head (Original) versus a linear classifier trained on the  
1354 frozen backbone (Retrained). The relative ranking of approximations remains consistent across both  
1355 settings.  
1356

Encoder	Approximation	Original Head Acc. $\uparrow$	Retrained Head Acc. $\uparrow$
DEiT-S	3 $\rightarrow$ 4, 9 $\rightarrow$ 11	72.44	$68.39 \pm 0.13$
	3 $\rightarrow$ 4, 9 $\rightarrow$ 10	77.25	$71.35 \pm 0.22$
	2 $\rightarrow$ 3	78.69	$73.19 \pm 0.19$
	10 $\rightarrow$ 11	78.78	$73.78 \pm 0.28$
	original	79.66	$73.85 \pm 0.39$
ViT-S	1 $\rightarrow$ 2	76.62	$70.32 \pm 0.38$
	2 $\rightarrow$ 3	78.25	$71.26 \pm 0.03$
	3 $\rightarrow$ 4	78.25	$71.40 \pm 0.22$
	4 $\rightarrow$ 5	77.66	$70.98 \pm 0.16$
	original	79.86	$73.24 \pm 0.13$

1363  
1364 As mentioned in the main paper, our primary evaluation involves training a new linear classifier on top  
1365 of the frozen model backbone to simulate a realistic transfer learning scenario. However, the original  
1366 papers for DEiT-S (Touvron et al., 2021) and ViT-S (Beyer et al., 2022) report performance using  
1367 the classification head that was part of the original pre-training.  
13681369 To confirm that our conclusions are robust and not an artifact of our evaluation protocol, we conducted  
1370 an additional set of experiments using the official, pre-trained classification heads from the original  
1371 model checkpoints. For consistency with our main experiments, we use the same number of samples  
1372 (500) for the approximation. In this setup, we do not train a new classifier; we simply evaluate the  
1373 accuracy of the frozen, approximated models using their original heads.  
13741375 The results, presented in Table 18, are fully consistent with the main conclusions of our paper. They  
1376 confirm that our block approximation method provides a favorable accuracy-efficiency trade-off, even  
1377 when evaluated with the original model heads. The relative drop in accuracy when approximating  
1378 different layers follows the same patterns observed in our primary experiments, reinforcing the  
1379 validity of our approach.  
13801381 A.2.6 COMPUTATIONAL EFFICIENCY VS. ACCURACY  
13821383 To quantify the effectiveness of different approximation methods, we analyze the trade-off between  
1384 downstream accuracy and computational cost. Figure 12 presents this analysis on a DiNo-B model  
1385 using both CIFAR-100F and ImageNet1k against three standard efficiency metrics: parameter  
1386 count, GFLOPs, and inference throughput. Across all metrics, the proposed linear translator (green)  
1387 establishes a more favorable Pareto frontier compared to the baseline identity-based approach (blue).  
1388 This indicates that for any given efficiency budget (e.g., a specific GFLOPs target), the linear translator  
1389 consistently yields a model with higher accuracy.  
13901391 A.2.7 ANALYSIS OF MISCLASSIFICATIONS  
13921393 In this section, we examine changes in per-class accuracy and misclassification patterns. As shown in  
1394 Figure 13, models behave differently at block approximations. DiNo-S remains remarkably stable  
1395 across blocks and classes, with the only degradation appearing for classes dog (when approximating  
1396 blocks 10 or 11) and deer (for block 10 approximation). ViT-S shows a similar drop for class dog  
1397 on its final block. Instead, the most noticeable hit occurs for class cat when the earlier blocks are  
1398 approximated. For DEiT-S, several mid-to-late block approximations improve accuracy for various  
1399 classes, whereas the very first block causes a clear relative decline in nearly every class. These  
1400 observations suggest strategies like preferring late-block approximation for DEiT-S, or reserving  
1401 extra samples for the linear transformation in order to recover the accuracy of difficult classes for the  
1402 model.  
1403

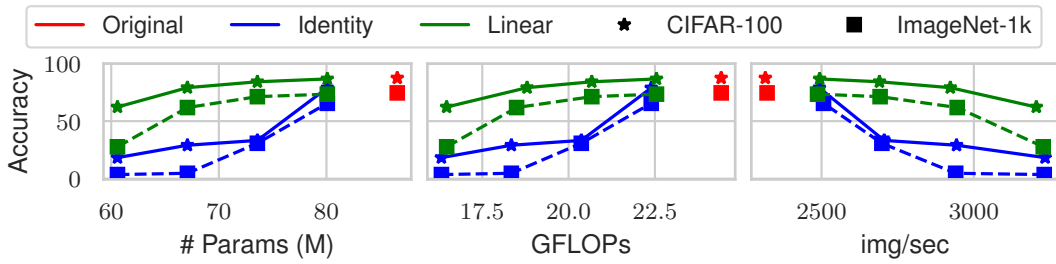


Figure 12: **Accuracy-efficiency trade-off for different approximation strategies.** Each subplot shows the accuracy against a different efficiency metric: the number of parameters (left), GFLOPs (center), and inference throughput (right). The image shows that the linear translator achieves a superior accuracy-efficiency trade-off.

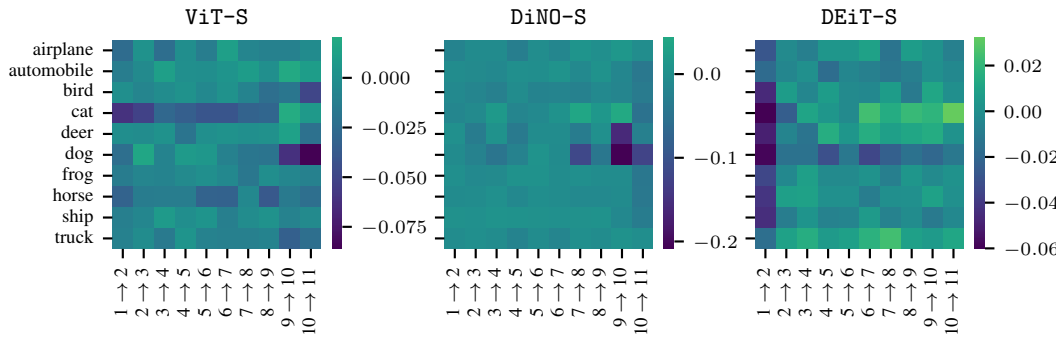


Figure 13: **Per-class accuracy delta on CIFAR-10 when a single block is approximated in ViT-S, DiNo-S and DeiT-S.** Cell values indicate the relative change in the accuracy with respect to the original model. Brighter (green) cells indicate an accuracy gain for the class, while darker (blue) cells indicate an accuracy drop.

In order to further investigate how the predictions change while approximating blocks, we plot the difference in the normalized confusion matrix before and after the approximation. In Figure 14, we show the delta confusion matrix for DeiT-S on CIFAR-100C. Also, here we can see how approximating the very first block makes the model puzzling and lose per-class accuracy (i.e., negative delta along the diagonal). On the other hand, approximating the last block acts as a regularizer, resulting in an overall gain in the per-class accuracy and, as a consequence, fewer misclassifications (negative deltas off-diagonal). This supports results shown in Figure 13 and Table 3.

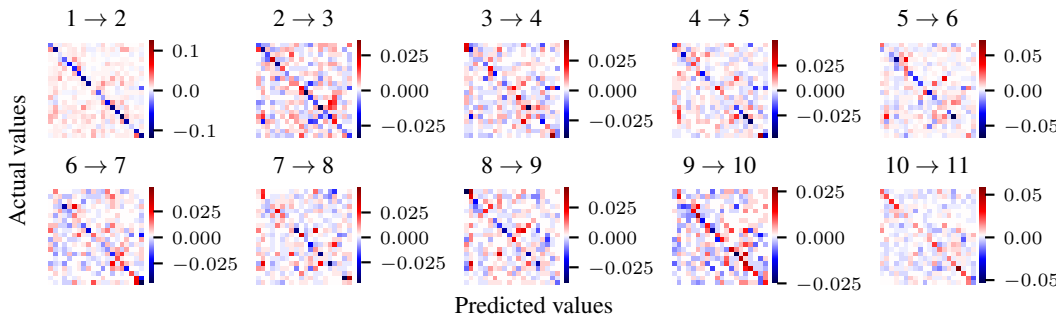


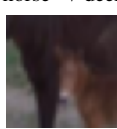
Figure 14: **Normalized relative confusion matrix when single blocks are approximated for DeiT-S on CIFAR-100C.** Diagonal cells capture the per-class change in accuracy, whereas off-diagonal cells capture changes in misclassifications between classes. Red (positive) values on the diagonal mean the approximation improves that class’s accuracy. Red off-diagonal values mean more misclassifications. Conversely, blue (negative) off-diagonal values indicate fewer misclassifications, and blue values on the diagonal indicate a drop in per-class accuracy.

1458 Additionally, Figure 15 shows representative CIFAR-10 images that become misclassified after  
 1459 approximating a block of ViT-S. The patterns we observe mirror the trends in Figures 13 and 14:  
 1460 when approximating earlier blocks, we observe many images belonging to class cat to be misclassified.  
 1461 Instead, when approximating later blocks, we observe images of the class dog to be misclassified.  
 1462 Together, these qualitative examples show that understanding these block-specific vulnerabilities  
 1463 allows us to steer the approximation procedure, informing choices about which blocks to approximate  
 1464 based on the observed impact on the final model’s class-wise performance.

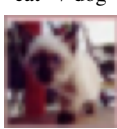
1465

1466

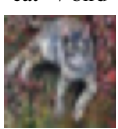
1467 horse → deer



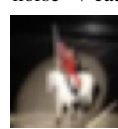
1468 cat → dog



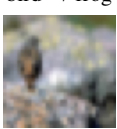
1469 1 → 2



1470 horse → cat



1471 bird → frog



1472

1473 bird → cat



1474 dog → cat



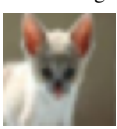
1475 6 → 7 automobile → truck



1476 dog → cat



1477 cat → dog

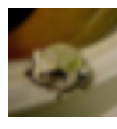


1478

1479 ship → airplane



1480 frog → cat



1481 10 → 11



1482 dog → cat



1483 truck → airplane



1484

1485 **Figure 15: Visualization of misclassified samples after approximating a block of ViT-S on**  
**CIFAR-10.** Images from CIFAR-10 whose label *flips from correct to incorrect* when specific  
 1486 blocks are approximated. The title reports the true class followed by the wrong prediction.

1487

1488

1489

1490

1491

1492

1493

1494

1495

1496

1497

1498

1499

1500

1501

1502

1503

1504

1505

1506

1507

1508

1509

1510

1511